CHALMERS
UNIVERSITY OF TECHNOLOGY

Safe and energy efficient predictive cruise control behind a slow-moving vehicle

Model predictive control for energy optimization

Master's thesis in Systems, Control and Mechatronics

Johnny Truong
Venkatraman Nagaraj

Department of Electrical Engineering
Chalmers University of Technology
Gothenburg, Sweden 2019

MASTER'S THESIS 2019

Safe and energy efficient predictive cruise control behind a slow-moving vehicle

Model predictive control for energy optimization

Johnny Truong
Venkatraman Nagaraj

Department of Electrical Engineering
CHALMERS UNIVERSITY OF TECHNOLOGY
Gothenburg, Sweden 2019

Safe and energy efficient predictive cruise control behind a slow-moving vehicle
Model predictive control for energy optimization
Johnny Truong
Venkatraman Nagaraj

Supervisor: Esteban Gelso, Volvo Group Trucks Technology
Examiner: Nikolce Murgovski, Department of Electrical Engineering

Master's Thesis 2019
Department of Electrical Engineering
Chalmers University of Technology
SE-412 96 Gothenburg
Telephone +46 31 772 1000

Cover: The Volvo Concept Truck [1]

Typeset in LaTeX
Gothenburg, Sweden 2019

Safe and energy efficient predictive cruise control behind a slow-moving vehicle
Model predictive control for energy optimization
Johnny Truong
Venkatraman Nagaraj
Department of Signal and Systems
Chalmers University of Technology

Abstract

The goal of this project is to develop an MPC (Model Predictive Control) algorithm which minimizes energy consumption for a controlled hybrid electrical vehicle while keeping a safe distance to a leading vehicle.
The algorithm consists of two main parts: speed prediction and optimization. An observer is first developed to estimate the power capability of the leading vehicle which is used to predict its driving behaviour. With the information of leading vehicle's driving, a reference speed trajectory can then be obtained for the controlled vehicle. The controller then minimizes the fuel consumption by finding the optimal control and state trajectories based on the reference speed and the road topography. The control signals include engine power, mechanical braking and power from electric machine. The states include traveling time, speed and battery energy.
The work was conducted in Matlab where the control-algorithm was tested in simulated driving scenario with measurement data of a heavy-duty leading vehicle driving on a known topography. The obtained results showed decreased fuel consumption with the hybrid electric vehicle compared to the conventional vehicle and manages to keep safe distance from another vehicle in front. However, the significant fuel reduction also exceeds results from previous works related to energy optimization of hybrid electrical vehicle. More measurement data is needed to further validate the performance of the control algorithm.

Keywords: Model Predictive Control, energy optimization, hybrid electrical vehicle

Acknowledgements

We would like to thank both our examiner, Nikolce Murgovski, and our supervisor, Esteban Gelso, for giving us the opportunity to work on this thesis. We would also like to thank the previous master thesis worker Mattias Hovgard who answered our questions and problems during our work.

Johnny Truong, Venkatraman Nagararaj,Gothenburg, June 2019

Contents

List of Figures

List of Tables

Variable	Unit	Description
α	rad	Road slope
s	m	Distance
t	s	Time
v	m/s	Vehicle speed
ω_{E}	rad/s	ICE speed
ω_{M}	rad/s	EM speed
T_{E}	Nm	ICE torque
T_{M}	Nm	EM torque
F_{E}	N	Engine force
F_{M}	N	EM force
F_{brk}	N	Mechanical braking force
F_{ebrk}	N	Engine braking force
F_{air}	N	Aero dynamic drag force
P_{E}	W	Engine power
P_{M}	W	EM power
P_{brk}	W	Mechanical braking power
P_{ebrk}	W	Engine braking power
P_{Td}	W	Total power loss
P_{Md}	W	Power loss from EM
E_{v}	J	Vehicle kinetic energy
E_{B}	J	Vehicle battery energy
λ_{B}	kg/J	Battery costate
μ	g/s	Fuel consumption
γ	-	gears
χ	-	ICE-state
u_{γ}	-	Gear control input
u_{χ}	-	ICE state control input
d_{LH}	m	Distance between leading and host vehicle

1

Introduction

Transportation of freight by road plays an important role in the modern global market. In our daily lives, products are seen everywhere which have been delivered by trucks from various industries. From 2007 to 2016, the total yearly freight being transported by road is approximately 75% in the EU [2] and about 70% in the US [3]. However, the high demand for transportation of freight by road leads to both environmental and financial issues. Despite representing a minority of vehicles on road in the EU, heavy trucks are responsible for approximately 30% of the CO2 emissions according to the International Council on Clean Transportation [4]. According to OECD [5], the statistics show that the amount of pollutants emitted by burning every gram of the heavy vehicle fuel and the effects of it are increasing.

To address this issue, one solution is to use a PCC (Predictive Cruise Control) which uses information of the road topography and surrounding traffic to predict the optimal speed of the truck [6]. For example, when the vehicle anticipates an uphill on the road that lies ahead, it can start decreasing its speed before reaching the top and then build up the speed when rolling downhill. Thus, more fuel is saved and less energy from applying the service brake is wasted.

Despite this, energy consumed through engine brake is inevitable and service brake may still need to be applied when traveling downhill. This solution can therefore be further improved by using an HEV (Hybrid Electrical Vehicle) which includes an additional power source, electric machine (EM). The HEV can use it for braking and converting the kinetic energy into electric energy, which is stored in a battery [7]. The stored energy can later be used for propulsion of the vehicle along with the power from internal combustion engine. This also allows the engine to be turned off during the periods of travel when the vehicle only relies on the electric machine, which reduces the fuel consumption even further.

However, the control strategy of HEV is more complex compared to a conventional one as it introduces more states and control signals which must be considered. The additional states include the battery energy and the state of engine (either on or off) and the additional control signals include the power from the electric machine and the input for deciding whether the engine should be on or off.

1.1 Background

There are several works related to energy optimization of conventional vehicle as well as HEV. One of the earlier projects worked on optimizing a heavy diesel truck with DP (Dynamic Programming) and MPC (Model Predictive Control) [8]. However, the downside with DP is that the computation time grows exponentially with the number of states and control signals [9]. This may be a problem for an HEV as more states and control signals must be considered compared to a conventional one.

In the project presented in [10], a control strategy for a hybrid long-haul truck was examined. In that project, an MPC was developed which consisted of three layers. The first layer optimized the energy of the two power sources in the vehicle by quadratic programming method. The second layer is solved by dynamic programming method where the integer states such as gear and the state of internal combustion engine were optimized. The obtained control signals and states were used for the current instance in the third layer. Their results showed that up to 4% of fuel could be saved while allowing the vehicle speed to vary around $\pm$ 5 km/h by minimizing the service braking.

Another work was a master thesis which presented the optimal control strategy for multiple HEVs traveling in platoon [11]. Their control strategy was a predictive CACC (Cooperative Adaptive Cruise Control) which utilized road information to optimize the vehicle speed and reduce the fuel consumption of the vehicle platoon. Their optimization problem was divided into smaller subproblems, which were solved in two layers. The first layer was the energy management which used convex optimization method and the second layer was the power management which used dynamic programming method. With their implemented control algorithm, their result showed that the average fuel consumption for each vehicle could be reduced by 10% with a platoon of four HEVs compared to a single HEV.

For this thesis, the predictive cruise control strategy of an HEV driving on a hilly terrain is further examined. However, in this project, an uncontrolled leading vehicle, driving in front of the controlled host vehicle is also considered. Therefore, the driving behaviour of the leading vehicle must also be predicted to ensure that the host vehicle keeps a safe distance to it.

Prediction of a leading vehicle by using MPC has previously been investigated in [12]. In their work, based on driving data obtained by experiments on an urban road with traffic signals, a prediction model of leading vehicle was created which estimated its acceleration/deceleration. By using the information of the predicted driving behaviour of the leading vehicle and the traffic states, their control algorithm could find optimal control input for the host vehicle while still keeping a safe distance to the leading vehicle.

However, when driving on a hilly terrain, the heavy-duty leading vehicle may drop speed due to its power limit. Therefore, an observer needs to be developed in this thesis. By collecting measurement data of the leading vehicle, the observer can then estimate the power limit of the leading vehicle which is used to determine its speed trajectory ahead.

1.2 Purpose

For this project, an MPC algorithm is developed to decrease the energy consumption of the controlled vehicle while ensuring a safe distance is kept to leading vehicle ahead. As it is assumed that there is no vehicle-to-vehicle communication, an observer needs to be developed which can estimate parameters such as mass and power to mass ratio of the leading vehicle to predict its driving behaviour.

1.3 Objective

The objective of this thesis is to develop an MPC algorithm to minimize the fuel consumption by using an already existing control algorithm as starting point for the development of MPC. The work is divided into the following main tasks:

- Design and implement an observer for the host vehicle in order to predict the behaviour of a leading vehicle, including its velocity trajectory.
- Implement an MPC algorithm.
- Evaluate the performance of the MPC algorithm.

1.4 Delimitations

Only one leading vehicle in front of the host vehicle is present in driving scenarios and perfect weather condition is assumed. Other traffic or obstacles are therefore not taken into consideration. The optimisation is only carried out on acceleration and braking. Therefore the steering of host vehicle is not taken into account. The computation time of the control algorithm is not considered.

1.5 Report outline

The report starts by describing the necessary theory in Chapter 2, which includes an overview of MPC and the physical model of the vehicle. In Chapter 3, the design of observer, problem formulation and control strategy are explained. In Chapter 4, the results obtained in the thesis are presented, which are discussed in Chapter 5. The report ends with the conclusion in Chapter 6.

2

Theory

In this chapter, the necessary theories to understand the thesis are presented. The basic concept of MPC is explained. The vehicle model is introduced as well.

2.1 Concept of MPC

MPC is a control method that has been applied in industries since late 70s [13]. It is also known as receding horizon control as its concept is based on the receding horizon idea. Unlike most controllers, MPC can effectively handle systems with multiple inputs and outputs which might be depended on each other [14]. Another big advantage with MPC is that constraints can be put for the control signals and the states.

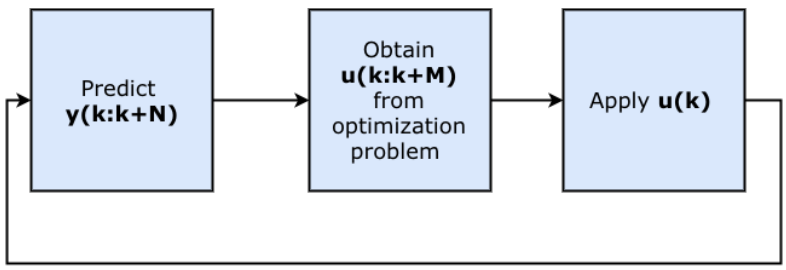

Figure 2.1: Simple block diagram of MPC.

The procedure of MPC shown in Figure 2.1 can be summarized by the following steps [14][15]:

1. At current sample instance k, the output signals $\mathbf{y}(k)$ are predicted with the process model for N instances ahead. The predicted output signals depend on the future control sequence over control horizon M.

2. Based on formulated cost function, objective and constraints for an optimization problem, the optimal control sequence is obtained and chosen.

3. The first element of the optimal control sequence is applied, and the rest is discarded. The controller then moves to next instance $(k + 1)$ and returns to

step 1 to repeat the procedure.

Normally, the length of control horizon M is set to be shorter than the length of prediction horizon N [15]. If that is the case, the rest of the control sequence after instance $k + M$ is set as either $\mathbf{u}(k + M)$ or 0.

2.2 Convex optimization problem

A standard form of convex optimization problem can be formulated as [15][16]

$$\begin{aligned} \text{minimize} \quad & f(\mathbf{x}) \\ \text{s.t.} \quad & g_i(\mathbf{x}) \leq 0, \quad i = 1, 2, .., m \\ & h_i(\mathbf{x}) = 0, \quad i = 1, 2, .., p \end{aligned} \tag{2.1}$$

where f is a cost function and $\mathbf{x} = \{x_1, x_2, ...x_n\}$ represents the optimization variables that should minimize f. The inequality and equality constraint functions are denoted by g_i and h_i, respectively. Both f and g_i are convex, and h_i are affine [15]. Another important property is that the local minimum is a global optimum.

These properties described for convex optimization problem are important when formulating our optimization problem later.

2.3 Vehicle model

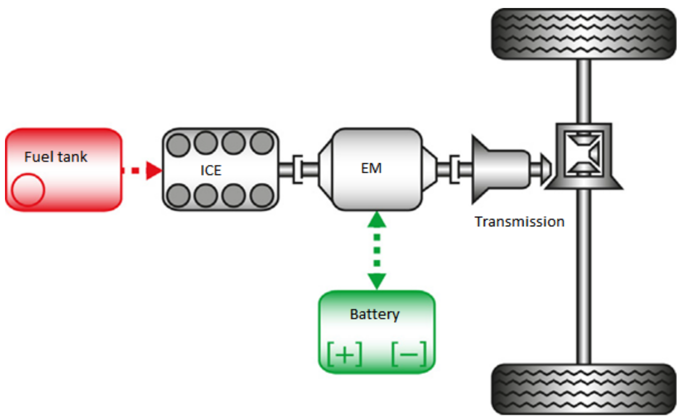

Figure 2.2: The powertrain configuration of host vehicle which shows gear box, final drive, ICE (Internal Combustion Engine), EM (Electric Machine) and their power sources. ICE and EM are connected to same gears.

The vehicle is modelled as a point mass that has the powertrain as illustrated in Figure 2.2, which is based on the HEV powertrain used in previous work by Department of Electrical Engineering at Chalmers University of Technology and Volvo Group Trucks Technology [10]. The powertrain is equipped with an ICE (Internal Combustion Engine) and an EM (Electrical Machine) which are connected to the same gear box and powered by fuel and battery, respectively. The clutch is responsible of switching between the EM and ICE. The vehicle model has three continuous states which are speed v, traveling distance s and battery energy E_{B}. The model also involves two real valued discrete states, which are the ICE state χ and gear number γ. Thus, the model is a hybrid system with mixed real- and integer states and control signals.

The longitudinal vehicle dynamic is modelled as

$$m\dot{v}(t) = F_{\mathrm{D}}(t) - mg\sin(\alpha) - F_{\mathrm{air}}(v) - F_{\mathrm{rol}}(\alpha) \tag{2.2}$$

where m is the mass of the host vehicle. The total traction force delivered to the wheels by ICE and EM is denoted by $F_{\mathrm{D}}(t)$. The gravitational force is denoted by g and α is the slope of the road depended on the travel distance $s(t)$, which in turn is depended on the travel time t. The force from the rolling resistance F_{rol} and air resistance F_{air} are described by

$$F_{\mathrm{rol}}(\alpha) = mgc_{\mathrm{r}}\cos(\alpha) \tag{2.3}$$

$$F_{\mathrm{air}}(v) = \frac{\rho_{\mathrm{a}} A_{\mathrm{f}} c_{\mathrm{d}}}{2} v^2(t) \tag{2.4}$$

where c_{r} is the rolling resistance coefficient, ρ_{a} is air density, A_{f} is frontal area of the host vehicle and c_{d} is the aerodynamic drag coefficient.

As shown in Figure 2.2, in this parallel configuration the EM and/or ICE transmits mechanical power to wheels. This mechanical power balance is described as

$$P_{\mathrm{E}}(t) + P_{\mathrm{M}}(t) + P_{\mathrm{brk}}(t) + P_{\mathrm{Ebrk}}(t) = F_{\mathrm{D}}(t)v(t) + P_{\mathrm{Td}}(\gamma, \chi, P_{\mathrm{E}}, P_{\mathrm{M}}, \mu_{\gamma}, \mu_{\chi}) \tag{2.5}$$

where $P_{\mathrm{Td}}(t)$ includes power loss due to shifts of gear and ICE and transmission losses. The braking powers P_{brk} and P_{Ebrk} represent the power consumed from mechanical brake and engine brake, respectively. The power used for propulsion from ICE is denoted by $P_{\mathrm{E}}(t)$, while the power from EM is denoted by $P_{\mathrm{M}}(t)$.

The electrical power balance is described as

$$P_{\mathrm{B}}(t) = P_{\mathrm{M}}(t) + P_{\mathrm{Md}}(v, P_{\mathrm{M}}) + P_{\mathrm{Bd}}(P_{\mathrm{B}}) + P_{\mathrm{A}}(t) \tag{2.6}$$

where $P_{\mathrm{B}}(t)$ is internal battery power, $P_{\mathrm{Md}}(v, P_{\mathrm{M}})$ and $P_{\mathrm{Bd}}(P_{\mathrm{B}})$ are power loss from EM and battery, respectively. The power consumed by auxiliary devices is denoted by $P_{\mathrm{A}}(t)$, but it is neglected for this HEV model.

The states of gear and ICE are defined as γ and χ, respectively, which can have the following values

$$\gamma \in \{1, ..., \gamma_{\max}\}, \qquad \chi \in \{0, 1\} \tag{2.7}$$

The values χ can have means it is either off (0) or on (1).

Their states for next time instance (γ^+, χ^+) are described by

$$\gamma^+ = \gamma + \mu_\gamma, \qquad \chi^+ = \chi + \mu_\chi \tag{2.8}$$

where $\mu_\gamma \in \{-1, 0, 1\}$ and $\mu_\chi \in \{-1, 0, 1\}$ are the switch commands for gear and state of ICE, respectively. When the gear is switched or the state of ICE is changed, additional fuel will be consumed, which are defined as the cost terms W_γ and W_χ, respectively.

2.3.1 ICE model

The fuel consumption of ICE, denoted by μ, as the function of engine speed and torque is formulated as

$$\mu(\omega_E(t), T_E(t)) = a_0 + a_1\omega_E(t) + a_2\omega_E^3(t) + a_3\omega_E^5(t) + a_4\omega_E(t)T_E(t) + a_5\omega_E(t)T_E^2(t) \tag{2.9}$$

where a_{0-5} are constants used for fitting. By fitting the model with measurements, the best fitted model is to put a_1 and a_2 as 0. Figure 2.3 illustrates the fuel consumption of ICE for different engine speeds and how well the model fits the measurements.

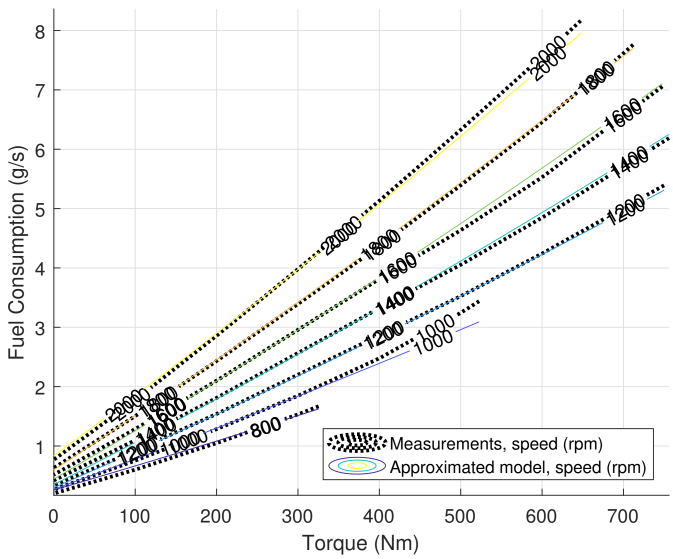

Figure 2.3: Fuel consumption is shown as the function of torque for various engine speeds. The measurements are shown in black and the fitted model is shown as contour. The numbers on the graphs represent the engine speed.

The speed and torque of ICE, denoted by $\omega_{\mathrm{E}}(t)$ and $T_{\mathrm{E}}(t)$ respectively, are described by

$$\omega(t) = v(t)r(\gamma) \tag{2.10a}$$

$$T_{\mathrm{E}}(t) = \begin{cases} \frac{F_{\mathrm{ICE}}(t)}{r(\gamma)\eta}, & \text{if } F_{\mathrm{ICE}}(t) \geq 0 \\ \frac{F_{\mathrm{ICE}}(t)\eta}{r(\gamma)}, & \text{if } F_{\mathrm{ICE}}(t) < 0 \end{cases} \Leftrightarrow T_{\mathrm{E}}(t) = \frac{1}{r(\gamma)} \max\left\{\frac{F_{\mathrm{ICE}}(t)}{\eta}, \eta F_{\mathrm{ICE}}(t)\right\} \tag{2.10b}$$

where η is the transmission efficiency from engine to wheel and F_{ICE} is the force delivered by ICE which can either be used for propulsion ($F_{\mathrm{ICE}} \geq 0$) or braking ($F_{\mathrm{ICE}} < 0$). ICE ratio, denoted by $r(\gamma)$, is defined as

$$r(\gamma) = \frac{r_{\mathrm{g}}(\gamma) r_{\mathrm{f}}}{R_{\mathrm{w}}} \tag{2.11}$$

where R_{w} is the radius of the wheels and r_{g} is the gear ratio. The gear ratio of the differential gears between ICE and EM is denoted by r_{f}.

The torque limits of ICE are illustrated in Figure 2.4, where they are plotted as a function of engine speed with the efficiency. The Figure also includes the maximum power that ICE can deliver.

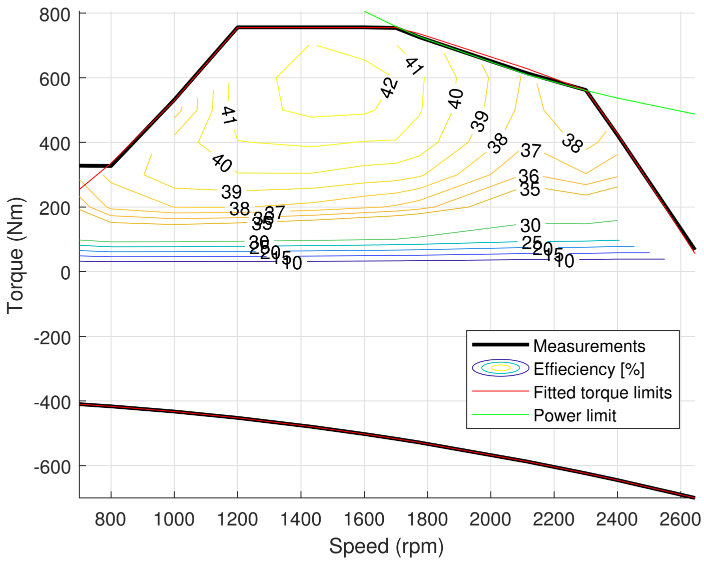

Figure 2.4: Torque limits and efficiency contour of ICE are shown as the function of engine speed. The original torque limits are in black and fitted torque limits are in red. The green line represents the maximum power delivered by ICE.

Converting engine speed and torque from Figure 2.4 to vehicle speed and force gives Figure 2.5 which illustrates the longitudinal force delivered by the engine to the wheels plotted as function of vehicle speed for different gear numbers.

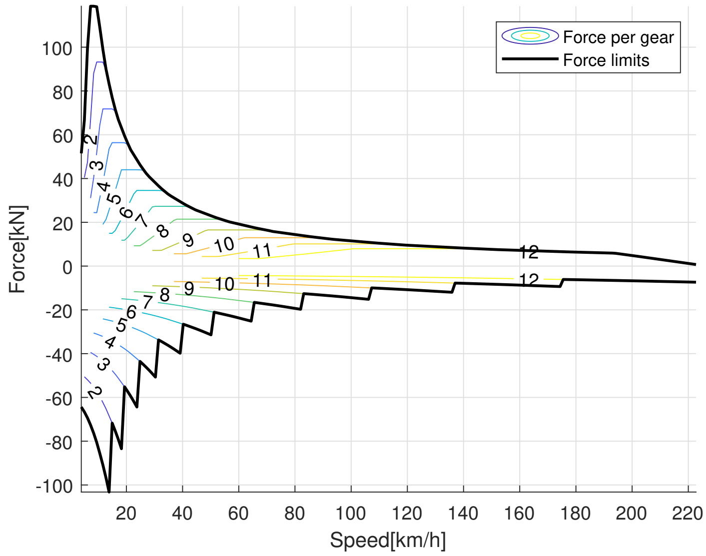

Figure 2.5: Longitudinal force that engine can deliver as function of vehicle speed for different gears.

From now on, the propulsion ($F_{\mathrm{ICE}} \geq 0$) and braking force ($F_{\mathrm{ICE}} < 0$) from ICE are referred as F_{E} and F_{Ebrk}, respectively.

The limit of $F_{\mathrm{E}}(t)$ can be described by several constraints. The first one is estimated as function of vehicle speed which is formulated as

$$F_{\mathrm{E}}(t) \leq \left(b_1 + b_2 v^2(t) r^2(\gamma)\right) r(\gamma)\eta \tag{2.12}$$

where b_1 and b_2 are constant coefficients. The second one is that $F_{\mathrm{E}}(t)$ should not exceed the maximum engine torque b_0

$$F_{\mathrm{E}}(t) \leq \ b_0 r(\gamma)\eta \tag{2.13}$$

The propulsion force is also limited by the maximum engine power P_{Emax}

$$F_{\mathrm{E}}(t) \leq \frac{\eta P_{\mathrm{Emax}}}{v(t)} \tag{2.14}$$

However, the limit for F_{E}, as shown in Figure 2.5, can be estimated by

$$F_{\mathrm{Emax}}(t) = F_0 + \frac{P_{\mathrm{Emax}}}{v(t)} \tag{2.15}$$

where F_0 is a constant used for fitting the limit. This limit can be used to determine whether the host vehicle is able to reach up to a certain desired speed or not. This is useful when predicting the speed trajectories of leading vehicle and host vehicle, which will be later described in Chapter 3.

The last constraint is that $F_{\mathrm{E}}(t)$ cannot be negative

$$F_{\mathrm{E}}(t) \geq 0 \tag{2.16}$$

The engine braking force F_{Ebrk} has two constraints. The first one is formulated as function of $v(t)$

$$F_{\mathrm{Ebrk}} \geq \left(c_1 + c_2 v(t)^2 r(\gamma)^2\right) \frac{r(\gamma)}{\eta} \tag{2.17}$$

where c_1 and c_2 are constants used to fit the model. The last one is that F_{Ebrk} cannot be positive

$$F_{\mathrm{Ebrk}} \leq 0 \tag{2.18}$$

Multiplying (2.12)-(2.16) and (2.17)-(2.18) with $v(t)$ yields the expressions of constraints in terms of power, which can also be further simplified as

$$P_{\mathrm{E}}(t) \leq \eta P_{\mathrm{Emax}} \tag{2.19a}$$

$$P_{\mathrm{E}}(t) \in \left[0, \min\left\{b_0, b_1 + b_2 r^2(\gamma) v^2(t)\right\}\right] r(\gamma)\eta v(t) \tag{2.19b}$$

$$P_{\mathrm{Ebrk}}(t) \in \left[\left(c_1 + c_2 v(t)^2 r(\gamma)^2\right), 0\right] \frac{r(\gamma)}{\eta} v(t) \tag{2.19c}$$

2.3.2 EM model

Since ICE and EM are connected to the same gear box, they share the same gearing ratio (r). This also means that EM has the same speed as ICE (w).

The expression of the torque of EM, denoted by $T_{\mathrm{M}}(t)$, depends on whether EM is used for propulsion or generation as described by

$$T_{\mathrm{M}}(t) = \begin{cases} \frac{F_{\mathrm{M}}(t)}{r(\gamma)\eta}, & \text{if } F_{\mathrm{M}}(t) \geq 0 \\ \frac{F_{\mathrm{M}}(t)\eta}{r(\gamma)}, & \text{if } F_{\mathrm{M}}(t) < 0 \end{cases} \Leftrightarrow T_{\mathrm{M}}(t) = \frac{1}{r(\gamma)} \max\left\{\frac{F_{\mathrm{M}}(t)}{\eta}, \eta F_{\mathrm{M}}(t)\right\} \tag{2.20}$$

where F_{M} is the force delivered by EM to the wheels. Torque limits are shown as the function of EM speed in Figure 2.6.

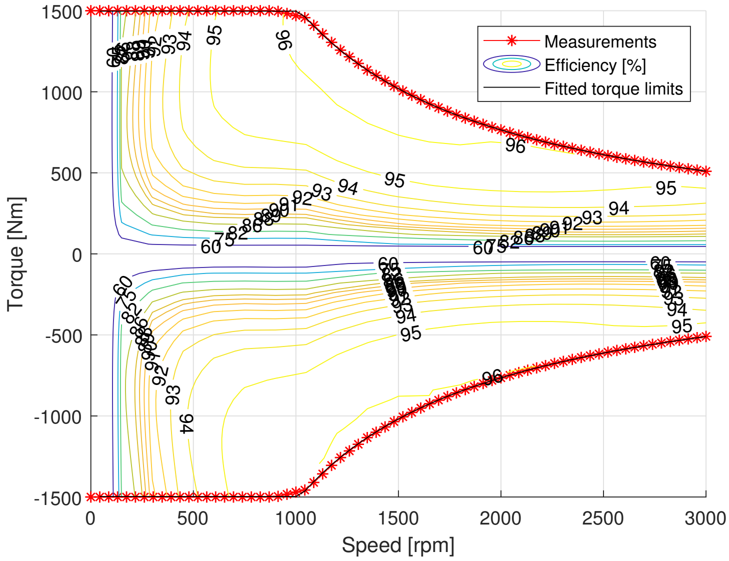

Figure 2.6: Torque limits as function of EM speed. The efficiency percentage is shown as contour, original torque limits are in black and fitted torque limits are in red.

The black lines represent the torque limits which are fitted by

$$T_{\text{Mmax}} = \min\left\{d_1, d_2 + \frac{d_3}{\omega(t)}\right\} \tag{2.21a}$$

$$T_{\text{Mmin}} = \max\left\{e_1, e_2 + \frac{e_3}{\omega(t)}\right\} \tag{2.21b}$$

where d_1, d_2, d_3, e_1, e_2 and e_3 are constants used for fitting. The limits of F_{M} are then expressed as

$$F_{\text{Mmax}}(t) = \min\left\{d_1, d_2 + \frac{d_3}{v(t)r(\gamma)}\right\} r(\gamma)\eta \tag{2.22a}$$

$$F_{\text{Mmin}}(t) = \max\left\{e_1, e_2 + \frac{e_3}{v(t)r(\gamma)}\right\} \frac{r(\gamma)}{\eta} \tag{2.22b}$$

Multiplying Equation (2.22) with $v(t)$ gives the expression of EM limits in terms of power

$$P_{\text{Mmax}} = \min\left\{d_1, d_2 + \frac{d_3}{v(t)r(\gamma)}\right\} r(\gamma)\eta v(t) \tag{2.23a}$$

$$P_{\text{Mmin}} = \max\left\{e_1, e_2 + \frac{e_3}{v(t)r(\gamma)}\right\} \frac{r(\gamma)v(t)}{\eta} \tag{2.23b}$$

The power losses of EM shown in Figure 2.7 is modelled as

$$P_{\mathrm{Md}}(t) = h_1\omega(t) + h_2\omega^3(t) + h_3\omega(t)|T_{\mathrm{M}}(t)| \tag{2.24}$$

where h_1, h_2 and h_3 are constants for fitted model.

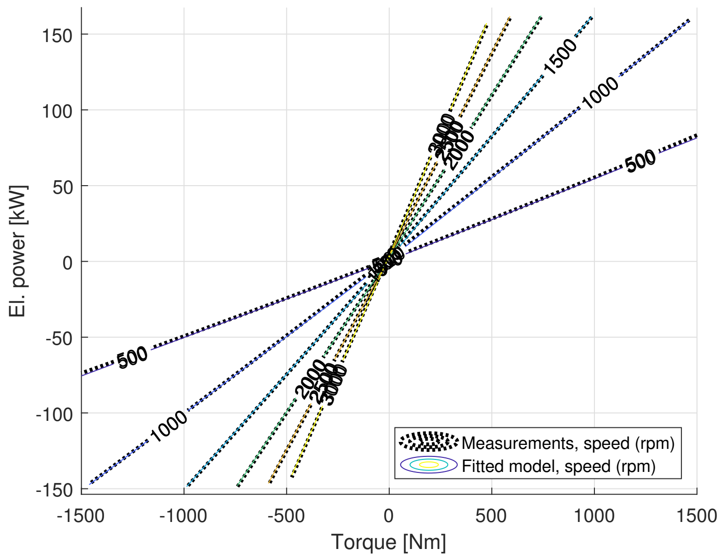

Figure 2.7: Electrical power consumed by EM is shown as the function of torque for various EM speeds. The original model is shown in black and the fitted model is shown as contour.

The total power consumed by EM is the sum of P_{Md} and P_{M}.

2.3.3 Battery model

Battery energy $E_{\mathrm{B}}(t)$ is regulated by the state

$$\dot{E}_{\mathrm{B}}(t) = -P_{\mathrm{B}}(t) \tag{2.25}$$

The state of charge, denoted by SOC, is defined according to Equation

$$\mathrm{SOC}(t) = \frac{E_{\mathrm{B}}(t)}{E_{\mathrm{Bmax}}} \tag{2.26}$$

where E_{Bmax} is the maximum energy capacity of the battery. The battery energy is limited by

$$E_{\mathrm{B}}(t) \in [\mathrm{SOC}_{\mathrm{min}}, \mathrm{SOC}_{\mathrm{max}}]E_{\mathrm{Bmax}} \tag{2.27}$$

where $\mathrm{SOC}_{\mathrm{min}}$ and $\mathrm{SOC}_{\mathrm{max}}$ are lower and upper bounds of SOC, respectively. The power loss of battery, denoted by P_{Bd}, is expressed as

$$P_{\mathrm{Bd}}(t) = \frac{R}{V_{\mathrm{oc}}^2} P_{\mathrm{B}}^2(t) \tag{2.28}$$

where V_{oc} represents constant open circuit voltage of the battery and R represents its constant resistance.

2.3.4 Safety constraint

A typical scenario of host vehicle driving on a road with leading vehicle in front of it can be seen in Figure 2.8 where there are both up and downhills.

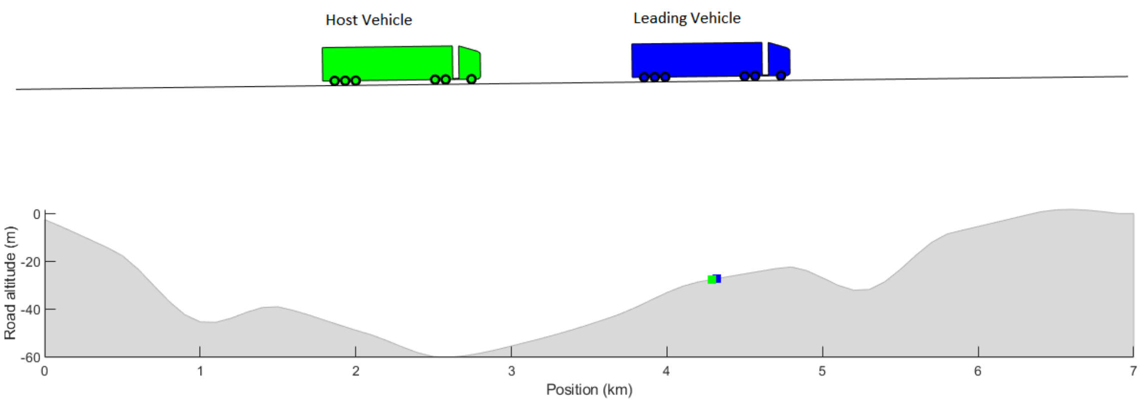

Figure 2.8: The leading vehicle and host vehicle driving on road with hills which is 7km long.

A safety constraint needs to be introduced to ensure that a safe distance can be kept between the host and leading vehicle. This can be formulated with their respective traveling times and add a time headway as described by

$$t \geq t_{\mathrm{L}} + \Delta t \tag{2.29}$$

where t_{L} and Δt denote the traveling time of leading vehicle and the time headway, respectively. The safety constraint can also be formulated in traveling distance as described by

$$d_{\mathrm{LH}} = s_{\mathrm{L}}(t) - s(t) \geq \Delta d \tag{2.30}$$

where s_{L} and s are the longitudinal positions of the leading and host vehicle, respectively. Thus, d_{LH} is the distance between the vehicles and Δd is the minimum required distance between them.

2.3.5 Aerodynamic drag model

Having a leading vehicle in front leads to an aerodynamic drag reduction of force for the host vehicle. The reduction depends on the distance between the vehicles, their respective speeds and geometries.

The aerodynamic drag reduction is modelled as follows,

$$F_{\mathrm{air}}(v, d_{\mathrm{LH}}) = F^0_{\mathrm{air}}(v(t))\,(1 - f_{\mathrm{d}}(d_{\mathrm{LH}}(t))) \tag{2.31a}$$

where F^0_{air} is the air resistance force experienced by host vehicle if there is no leading vehicle ahead. The air resistance force in turn is described by

$$F^0_{\mathrm{air}}(v) = \frac{\rho_{\mathrm{a}} A_{\mathrm{f}} c_{\mathrm{d}}}{2} v(t) \tag{2.31b}$$

The expression of aerodynamic drag coefficient for host vehicle, denoted by $f_{\mathrm{d}}(d_{\mathrm{LH}})$, is described by

$$f_{\mathrm{d}}(d_{\mathrm{LH}}) = a_{1_{\mathrm{LH}}}\exp(-b_{1_{\mathrm{LH}}} d_{\mathrm{LH}}(t)) + a_{2_{\mathrm{LH}}}\exp(-b_{2_{\mathrm{LH}}} d_{\mathrm{LH}}(t)) \tag{2.32}$$

where the coefficients $a_{1\mathrm{LH}}$, $a_{2\mathrm{LH}}$, $b_{1\mathrm{LH}}$ and $b_{2\mathrm{LH}}$ are adjusted by fitting measurement data. Figure 2.9 illustrates the drag reduction of host vehicle where there is one leading vehicle present. The aerodynamic drag model described by Equation (2.32) fits the measurement data in Figure 2.9. It can be seen that the longer the distance between the vehicles is, the less air drag reduction f_{d} there is.

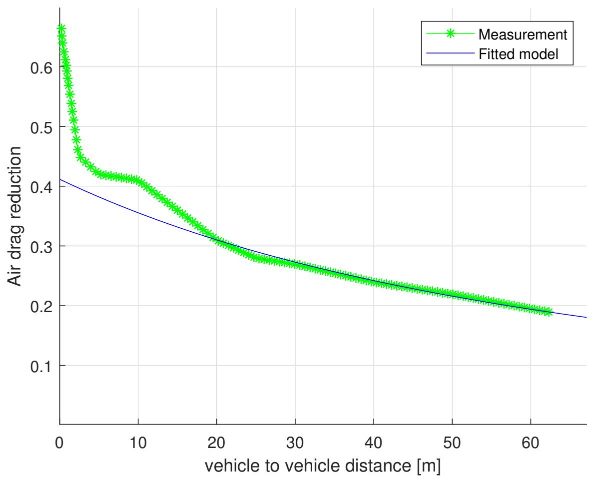

Figure 2.9: Comparison between measurement data and fitted model of aerodynamic drag reduction $f_{\mathrm{d}}(d_{\mathrm{LH}})$.

3

Methods

This chapter describes the procedure for predicting the behaviour of leading vehicle and the control strategy used to optimize the fuel consumption of the host vehicle.

3.1 Overview

The controller is a PCC (Predictive Cruise Controller), which estimates the optimal trajectories [17][18][19] for the states and control signals of the host vehicle in order to minimize its fuel consumption. For this project, the controller is extended to an MPC where the control horizon M is set as the same length as the prediction horizon N. At current time instance t_0, the optimal trajectories are predicted N instances ahead. Thus, the final instance of the predicted horizon becomes

$$t_{\mathrm{f}} = t_0 + N \tag{3.1}$$

The states are the speed v, traveled distance s, battery energy E_{B}, gear γ and ICE state χ. The control signals are the powers P_{M}, P_{E} P_{Ebrk}, P_{brk}, gear selection u_γ and ICE selection u_χ. A constant cruising speed $\bar{v}$ is assumed to be set for the host vehicle.

However, when the road topography and the behaviour of leading vehicle are taken into consideration, it might not be possible to maintain the set cruising speed for certain instances. To predict how the leading vehicle drives, some of its parameters need to be estimated first, including its power to mass-ratio, by a leading vehicle observer. The estimated parameters can then be used to determine if the cruising speed of leading vehicle, denoted by $\bar{v}_{\mathrm{L}}$, is feasible or not (more on this in Section 3.6.1). Based on the road topography and the predicted driving of leading vehicle, a reference speed trajectory of host vehicle can then be obtained.

With the reference speed trajectory and a formulated optimization problem, the controller estimates the optimal trajectories for the states and control signals of host vehicle, while ensuring a safe distance to the leading vehicle is kept. Only the first elements of the respective trajectories are applied. The rest is then discarded and MPC performs an update with the whole procedure repeated at next instance.

3.2 Formulation of optimization problem

The optimization problem that the controller should solve is formulated as

$$\begin{aligned} &\text{minimize} \quad J = \int_{t_0}^{t_\mathrm{f}} (\chi(t)\mu(\cdot) + W_\gamma(\cdot) + W_\chi(\cdot))dt \\ &\text{subject to} \end{aligned} \tag{3.2a}$$

$$P_\mathrm{E}(t) + P_\mathrm{M}(t) + P_\mathrm{brk}(t) + P_\mathrm{Ebrk}(t) = F_\mathrm{D}(t)v(t) + P_\mathrm{Td}(\cdot) \tag{3.2b}$$

$$P_\mathrm{B}(t) = P_\mathrm{M}(t) + P_\mathrm{Md}(v, P_\mathrm{M}) + P_\mathrm{Bd}(P_\mathrm{B}) \tag{3.2c}$$

$$m\dot{v}(t) = F_\mathrm{D}(t) - F_\mathrm{air}(v, d_\mathrm{LH}) - mg(\sin(\alpha) + c_\mathrm{r}\cos(\alpha)) \tag{3.2d}$$

$$\dot{E}_\mathrm{B}(t) = -P_\mathrm{B}(t) \tag{3.2e}$$

$$s(t_0) = s_0, \quad s(t_\mathrm{f}) = s_\mathrm{f} \tag{3.2f}$$

$$\dot{s}(t) = v(t) \tag{3.2g}$$

$$v(t_0) = v_0 \tag{3.2h}$$

$$v(t) \in [v_\mathrm{min}(t), v_\mathrm{max}(t)] \tag{3.2i}$$

$$t \in [t_0, t_\mathrm{f}] \tag{3.2j}$$

$$t_\mathrm{f} - t_0 \leq t_\mathrm{max} \tag{3.2k}$$

$$P_\mathrm{E}(t) \leq \eta P_\mathrm{Emax} \tag{3.2l}$$

$$P_\mathrm{E}(t) \in \left[0, \min\left\{b_0, b_1 + b_2 r^2(\gamma)v^2(t)\right\}\right] r(\gamma)\eta v(t) \tag{3.2m}$$

$$P_\mathrm{M}(t) \in [P_\mathrm{Mmin}(v,\gamma), P_\mathrm{Mmax}(v,\gamma)] \tag{3.2n}$$

$$P_\mathrm{brk}(t) \leq 0 \tag{3.2o}$$

$$P_\mathrm{Ebrk}(t) \in \left[\left(c_1 + c_2 v(t)^2 r(\gamma)^2\right), 0\right] \frac{r(\gamma)}{\eta} v(t) \tag{3.2p}$$

$$E_\mathrm{B}(t_0) = E_\mathrm{B0}, \quad E_\mathrm{B}(t_\mathrm{f}) \geq E_\mathrm{Bf} \tag{3.2q}$$

$$E_\mathrm{B}(t) \in [\mathrm{SOC}_\mathrm{min}, \mathrm{SOC}_\mathrm{max}]E_\mathrm{Bmax} \tag{3.2r}$$

$$\chi^+(t) = \chi(t) + u_\chi(t), \quad \chi(t) \in X, \quad u_\chi(t) \in U_\chi \tag{3.2s}$$

$$\gamma^+(t) = \gamma(t) + u_\gamma(t), \quad \gamma(t) \in \Gamma, \quad u_\gamma(t) \in U_\gamma \tag{3.2t}$$

$$s_\mathrm{L}(t) \geq s(t) + \Delta d \tag{3.2u}$$

The terms W_γ and W_χ are the penalties added for changing gear-and ICE-state, respectively. This is to avoid shifting too frequently, as it is not desirable. Note that μ is multiplied with χ to ensure that fuel consumption only occurs when ICE is on.

Since the constant efficiency η already includes the losses from the transmission, only the losses from shifting gear and ICE-state are included in P_{Td}.

This optimization problem has both real valued and integer states and variables, making it computationally heavy to solve. Therefore, the problem is divided into two layers, which will be later described in Section 3.3.

Equation (3.2k) ensures that even if v deviates from the reference speed v_{r}, the host vehicle should still be able to complete the horizon within the same time frame $t_{\max}$ as if it would have driven with v_{r}.

3.3 Control scheme

The optimization problem in Equation (3.2) is solved by two layers, which is illustrated in Figure 3.1. This is a common method, which has been done in previous works [20][21][9]. Both layers minimize the cost function given in Equation (3.2a), but with different methods and in regards to different states/control signals. The top and bottom layer are referred as energy and power management, respectively.

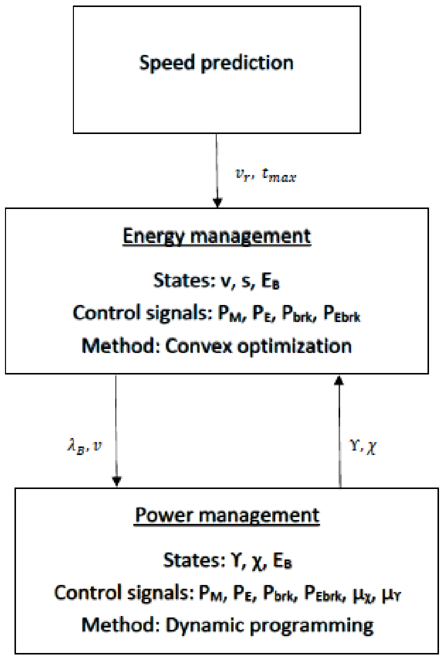

Figure 3.1: The control scheme divided into two layers, energy and power management. Energy management estimates the optimal trajectories for v and λ_{B}, which are then sent to the power management. The power management in turn estimates the optimal trajectories for γ and χ, which are then sent to energy management to estimate its optimal state and control trajectories again.

After obtaining the reference speed trajectory v_r, the energy management solves the optimization problem with convex optimization to estimate the optimal trajectories for the states v, t and E_B as well as the control signals P_E, P_M, P_Ebrk and P_brk. The energy management also estimates the battery costate trajectory λ_B, which will be further described in Section 3.8. Both v and λ_B are then sent to the power management.

The power management estimates the optimal trajectories for the states E_B,γ and χ as well for the control signals, including gear selection u_γ and ICE-selection u_χ, by using dynamic programming. The energy management then receives γ and χ to solve the optimization problem and send v and λ_B to the power management again.

This process is repeated until a solution converges or until a maximum number of iteration has been reached.

3.4 Variable change

As data of road topography are usually given in space coordinates, it is more beneficial to work in space domain than in time domain. Therefore, the travel distance s replaces the travel time t as the independent variable. Rewriting from time domain to space domain should be done according to

$$t'(s) = \frac{dt}{ds} = \frac{1}{v(s)} \tag{3.3}$$

In space domain, it is easier to work with forces and kinetic energy instead of power and velocity. Therefore, the forces are given as

$$F_\mathrm{E} = \frac{P_\mathrm{E}(s)}{v(s)}, F_\mathrm{M} = \frac{P_\mathrm{M}(s)}{v(s)}, F_\mathrm{B} = \frac{P_\mathrm{B}(s)}{v(s)}, F_\mathrm{brk} = \frac{P_\mathrm{brk}(s)}{v(s)}, F_\mathrm{Ebrk} = \frac{P_\mathrm{Ebrk}(s)}{v(s)} \tag{3.4}$$

and the speed $v(s)$ is replaced with kinetic energy $E_\mathrm{v}(s)$ according to

$$E_\mathrm{v}(s) = \frac{mv^2(s)}{2} \tag{3.5}$$

With the variable change, the equation of motion from (2.2) is rewritten as

$$E'_\mathrm{v}(s) = mv'(s)v(s) \tag{3.6}$$

The final instance for the predicted horizon described in Equation (3.1) is also modified as

$$s_\mathrm{f} = s_0 + S_\mathrm{p} \tag{3.7}$$

where s_0 and S_p are the current instance and prediction horizon in space domain, respectively.

3.5 Linearization and approximations

By changing the variables, the constraints which had $1/v(s)$ will instead have $1/\sqrt{E_\mathrm{v}(s)}$, as seen in the function $f_t(E_\mathrm{v})$ described by

$$f_t(E_\mathrm{v}) = \frac{1}{v(s)} = \sqrt{\frac{m}{2E_\mathrm{v}(s)}} \tag{3.8}$$

where t denotes the expression in Equation (3.3). However, as those constraints are not convex, this is an issue for the energy management which uses convex optimization to solve the optimization problem. Therefore, the function needs to be linearized around the reference kinetic energy $\hat{E}_\mathrm{v}(s)$, which is the kinetic energy when the host vehicle drives with reference speed v_r. The linearization is described as

$$f_t^{\mathrm{lin}}(E_\mathrm{v}) = f_t(\hat{E}_\mathrm{v}(s)) + \left.\frac{\partial f_t}{\partial E_\mathrm{v}}\right|_{\hat{E}_\mathrm{v}} \Delta E_\mathrm{v}(s) \tag{3.9}$$

where $\Delta E_\mathrm{v}(s) = E_\mathrm{v}(s) - \hat{E}_\mathrm{v}(s)$.

3.5.1 ICE model

The fuel consumption μ is modified as

$$\tilde{\mu}(\cdot) = \frac{\mu(\cdot)}{v(s)} \tag{3.10}$$

In the beginning of each MPC-update, the gear trajectory has not been updated before solving the optimization problem in energy management (more details described in Section 3.3). This might lead to infeasible force delivered by ICE, as the current gear trajectory may not have been properly selected to provide sufficient force to reach up to the updated speed v. Therefore, F_E is reformulated and expressed as

$$F_\mathrm{E}(s) = \chi(s)F_{\mathrm{E1}}(s) + F_{\mathrm{E2}}(s) \tag{3.11}$$

where F_{E1} is the force from current gear trajectory and F_{E2} is an abstract force which can be delivered from any other chosen gear and state of ICE. The ICE-state χ is multiplied with F_{E1} to ensure that the force is only available when ICE is on. If F_{E1} is not sufficient to fulfill the constraint in Equation (2.12), F_{E2} is applied to cover up the rest of F_{E}.

The constraint for F_{E} from (2.12) is subsequently reformulated as

$$\chi F_{\mathrm{E1}}(s) + F_{\mathrm{E2}}(s) \leq \eta P_{\mathrm{Emax}} \sqrt{\frac{m}{2E_{\mathrm{v}}(s)}} \tag{3.12}$$

This however needs to be linearized as

$$\chi F_{\mathrm{E1}}(s) + F_{\mathrm{E2}}(s) \leq \eta P_{\mathrm{Emax}} f_t^{\mathrm{lin}}(E_{\mathrm{v}}(s)) \tag{3.13}$$

The constraint for F_{E1} is now described by Equation

$$F_{\mathrm{E1}}(s) \in \left[0, \min\left\{b_0, b_1 + \frac{2b_2}{m} E_{\mathrm{v}}(s) r^2(\gamma)\right\}\right] r(\gamma)\eta \tag{3.14}$$

The constraint for braking force F_{Ebrk} is also reformulated as

$$F_{\mathrm{Ebrk}}(s) \in \left[\left(c_1 + \frac{2c_2}{m} E_{\mathrm{v}}(s) r^2(\gamma)\right), 0\right] \frac{r(\gamma)}{\eta} \tag{3.15}$$

3.5.2 EM model

The wheel force from EM has the constraints described by

$$F_{\mathrm{Mmax}}(E_{\mathrm{v}}) = \min\left\{d_1, d_2 + \frac{d_3}{r(\gamma)} \sqrt{\frac{m}{2E_{\mathrm{v}}(s)}}\right\} r(\gamma)\eta \tag{3.16a}$$

$$F_{\mathrm{Mmin}}(E_{\mathrm{v}}) = \max\left\{e_1, e_2 + \frac{e_3}{r(\gamma)} \sqrt{\frac{m}{2E_{\mathrm{v}}(s)}}\right\} \frac{r(\gamma)}{\eta} \tag{3.16b}$$

However, these Equations are not convex. Therefore, they are linearized as described by Equation (3.9), which gives

$$F_{\mathrm{Mmax}}(E_{\mathrm{v}}) = \min\left\{d_1, d_2 + \frac{d_3}{r(\gamma)} f_t^{\mathrm{lin}}(E_{\mathrm{v}}(s))\right\} r(\gamma)\eta \tag{3.17a}$$

$$F_{\mathrm{Mmin}}(E_{\mathrm{v}}) = \max\left\{e_1, e_2 + \frac{e_3}{r(\gamma)} f_t^{\mathrm{lin}}(E_{\mathrm{v}}(s))\right\} \frac{r(\gamma)}{\eta} \tag{3.17b}$$

The force losses from EM, denoted by F_{Md}, is described by

$$F_{\mathrm{Md}}(s) = h_1 r(\gamma) + \frac{2h_2 r^3(\gamma)}{m} E_{\mathrm{v}}(s) + h_3 \left| \max \left\{ \frac{F_{\mathrm{M}}(s)}{\eta}, \eta F_{\mathrm{M}}(s) \right\} \right| \tag{3.18}$$

3.5.3 Battery model

The energy battery is reformulated as

$$E'_{\mathrm{B}}(s) = -F_{\mathrm{B}}(s) \tag{3.19}$$

Force dissipation from battery, denoted by $F_{\mathrm{Bd}}(s)$, is described by

$$F_{\mathrm{Bd}}(s) = \frac{R}{V_{\mathrm{oc}}^2} \sqrt{\frac{2E_{\mathrm{v}}(s)}{m}} F_{\mathrm{B}}^2(s) \approx \frac{R}{V_{\mathrm{oc}}^2} \sqrt{\frac{2\hat{E}_{\mathrm{v}}(s)}{m}} F_{\mathrm{B}}^2(s) \tag{3.20}$$

As seen in the Equation, the expression is simplified by replacing $E_{\mathrm{v}}(s)$ with $\hat{E}_{\mathrm{v}}(s)$. This is to avoid multiplication of different variables, which would otherwise have made it into a non-convex optimization problem.

3.5.4 Aerodynamic drag model

The air resistance force F_{air} in Equation (2.31a) is rewritten in space domain as

$$F_{\mathrm{air}}(E_{\mathrm{v}}, d_{\mathrm{LH}}) = F_{\mathrm{air}}^0(E_{\mathrm{v}}(s))\,(1 - f_{\mathrm{d}}(d_{\mathrm{LH}}(s))) \tag{3.21}$$

The function $f_{\mathrm{d}}(d_{\mathrm{LH}}(s))$ is however both nonlinear and non-convex. Therefore, it is linearized around the distance between the vehicles estimated with their reference speeds, denoted by $\hat{d}_{\mathrm{LH}}(s))$, as seen in

$$F_{\mathrm{air}}^{\mathrm{lin}}(E_{\mathrm{v}}, d_{\mathrm{LH}}) = c_{\mathrm{a}} E_{\mathrm{v}}(s) \left(1 - f_{\mathrm{d}}(\hat{d}_{\mathrm{LH}}(s))\right) - c_{\mathrm{a}} \hat{E}_{\mathrm{v}}(s) \left(d_{\mathrm{LH}}(s) - \hat{d}_{\mathrm{LH}}(s)\right) \left.\frac{\partial f_{\mathrm{d}}}{\partial d_{\mathrm{LH}}}\right|_{\hat{d}_{\mathrm{LH}}} \tag{3.22}$$

The distance between leading and host vehicle, denoted by d_{LH}, is calculated as

$$d_{\mathrm{LH}}(s) = x_{\mathrm{L}}(s) - x(s) \tag{3.23}$$

where $x_{\mathrm{L}}(s)$and $x(s)$ are the longitudinal positions of leading and host vehicles, respectively, as function of s. By assigning $x(s) = s$, the leading vehicle position can be given as

$$x'_{\mathrm{L}}(s) = \frac{v_{\mathrm{L}}(s)}{v(s)} \tag{3.24}$$

Assuming that leading vehicle speed $v_{\mathrm{L}}(s)$ does not deviate much from its desired speed $\bar{v}_{\mathrm{L}}$, Equation (3.24) is simplified as

$$x_{\mathrm{L}}^{'}(s) = \bar{v}_{\mathrm{L}} t'(s) \tag{3.25}$$

By integrating Equation (3.25), x_{L} can then be described by Equation

$$x_{\mathrm{L}}(s) = \bar{v}_{\mathrm{L}}(t(s) - t_0) \tag{3.26}$$

Equation (3.23) can therefore be rewritten as

$$d_{\mathrm{LH}}(s) = \bar{v}_{\mathrm{L}}(t(s) - t_0) - s \tag{3.27}$$

3.6 Reference speed of host vehicle

Before solving the optimization problem, a reference speed trajectory of the host vehicle, v_{r}, needs to be obtained. In this section, the process for predicting v_{r} is described. Only the force delivered by ICE is considered to make the comparison of host vehicle as CV (Conventional Vehicle) and as HEV more fair.

3.6.1 Leading vehicle observer

The importance of maximum engine power was previously described in Section 2.3.1. However based on the equation of motion, another term is also unknown which is the ratio of aerodynamic drag and mass. Therefore, rather than the maximum longitudinal force F_{Lmax}, the limit that needs to be estimated is the acceleration limit a_{max} described by

$$a_{\mathrm{max}} = \frac{F_{\mathrm{Lmax}} - F_{\mathrm{Lair}}}{m_{\mathrm{L}}} = \frac{F_{\mathrm{L0}}}{m_{\mathrm{L}}} + \frac{P_{\mathrm{Lmax}}}{m_{\mathrm{L}} \cdot v_{\mathrm{L}}(s)} - \frac{c_{\mathrm{La}} \cdot v_{\mathrm{L}}^2(s)}{2m_{\mathrm{L}}} \tag{3.28}$$

where m_{L} is the mass of leading vehicle, F_{L0} is a constant force parameter to fit the limit, c_{La} is its aerodynamic drag coefficient and P_{Lmax} is its maximum engine power. Thus, the scalar parameters that need to be obtained are $l_0 = \frac{F_{\mathrm{L0}}}{m_{\mathrm{L}}}$, $l_1 = \frac{P_{\mathrm{Lmax}}}{m_{\mathrm{L}}}$ and $l_2 = \frac{c_{\mathrm{La}}}{2m_{\mathrm{L}}}$. With the measurement data (including traveling time, speed of leading vehicle as well as the slope of the road topography), the measured acceleration capabilities a_{meas} can be calculated according to

$$a_{\mathrm{meas}} = \frac{F_{\mathrm{L}}}{m_{\mathrm{L}}} - \frac{c_{\mathrm{a}} \cdot v_{\mathrm{L}}^2(s)}{2m_{\mathrm{L}}} = \dot{v_{\mathrm{L}}}(s) + g \cdot (\sin\alpha + c_{\mathrm{r}}\cos\alpha) \tag{3.29}$$

To illustrate a_{meas}, an example is shown in Figure 3.2. In this Figure, a_{meas} have been calculated by using measurement data collected with sample distance of 80m from a vehicle which has traveled for 20km.

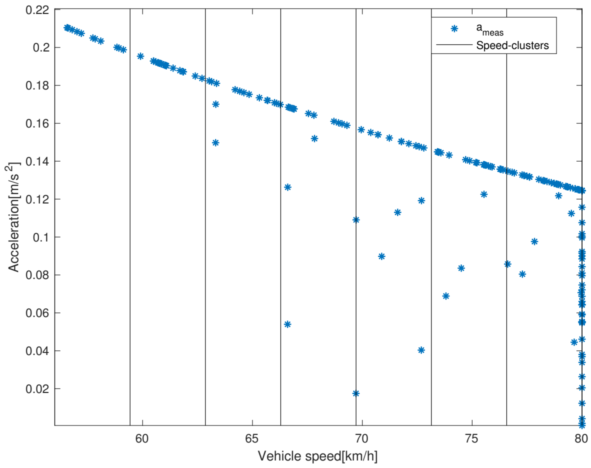

Figure 3.2: Acceleration as function of vehicle speed. The blue star points represent a_{meas} and the black lines represent the speed-clusters.

Since the a_{meas}-values which operate on a_{max} are relevant for estimating a_{max}, only the highest values of a_{meas} are needed. Therefore, a_{meas} are grouped based on their speeds by several shorter but equally long intervals referred as speed-clusters. In Figure 3.2, the number of speed-clusters is seven.

For each speed-cluster, the highest a_{meas}-value is then saved and the rest is discarded. The limit a_{max} can then be estimated by solving LP (Linear Programming) [22] with the cost function formulated as

$$\begin{aligned} &\min_{l_0,l_1,l_2} \quad \int_0^{v_{\mathrm{Lmax}}} a_{\mathrm{Lmax}}(v_{\mathrm{L}}) dv_{\mathrm{L}} = \sum_{j=1}^{K} a_{\mathrm{max}}(v_{\mathrm{L}j}) = l_0 \cdot K + l_1 \sum_{j=1}^{K} \frac{1}{v_{\mathrm{L}j}} - l_2 \sum_{j=1}^{K} {v_{\mathrm{L}j}}^2 \\ &\text{s.t.} \quad a_{\mathrm{max}}(v_{\mathrm{L}j}) \geq a_{\mathrm{meas}_j}, \qquad j = 1, 2, .., K \end{aligned} \tag{3.30}$$

where v_{Lmax} denotes the highest measured vehicle speed collected and K denotes the number of relevant points. From what has been previously been studied, a_{max} should be a monotonically decreasing function. Therefore, boundaries for l_0,l_1 and l_2 are put to ensure that the estimated a_{max} does not get an unexpected shape such as concave function.

After the vehicle parameters l_0, l_1 and l_2 have been obtained from the observer, they can then be used to estimate a_{max} as described by Equation (3.28). The estimated a_{max} is seen in Figure 3.3.

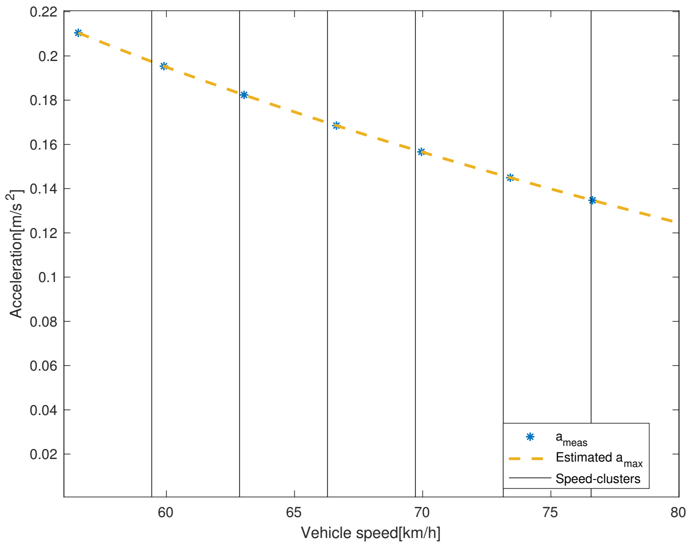

Figure 3.3: Acceleration as function of vehicle speed. The blue star points represent a_{meas}.

3.6.2 Noise disturbance

For the example described in Figures 3.2 and 3.3, simulated measurements without noise disturbance were used. However, real measurement data contains noise disturbance which can severely affect the results.

To reduce the impact of it, some measures need to be taken. The measured speed is first smoothed with Savitzky-Golay filter [23] before a_{meas} are calculated. A limit for a_{meas} as function of vehicle speed is also introduced in observer to further reduce the noise. If an a_{meas} exceeds this limit, it will be removed and not be considered when a_{max} is estimated. In the observer, a limit for jerk (derivative of acceleration in regards to time) is also put to ensure that one a_{meas}-point does not deviate too much from other points.

Figure 3.4 shows an example of a_{meas}-points collected as function of vehicle speed and where there are points which deviate significantly from the rest, which are considered as outliers. The black line represents the highest possible a_{max}. In this example, there are three a_{meas}-points which lie above that limit. There is also another a_{meas}-point which lies just below the limit but deviates significantly from the other points.

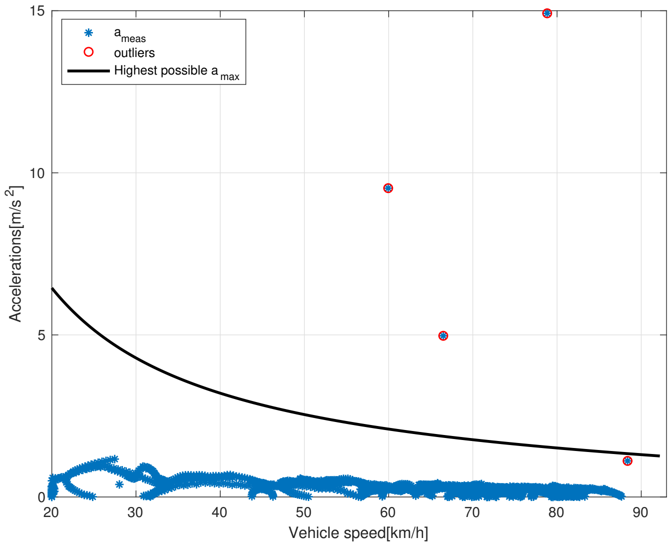

Figure 3.4: Acceleration a_{meas} as function of vehicle speed. The black line is the highest possible a_{max}. The points with red circles are considered as outliers.

With the approach to reduce noise impact, the three points above the limit are neglected. The point just below it is solved with the limit put for jerk. Figure 3.5 shows the result of filtering out the outliers.

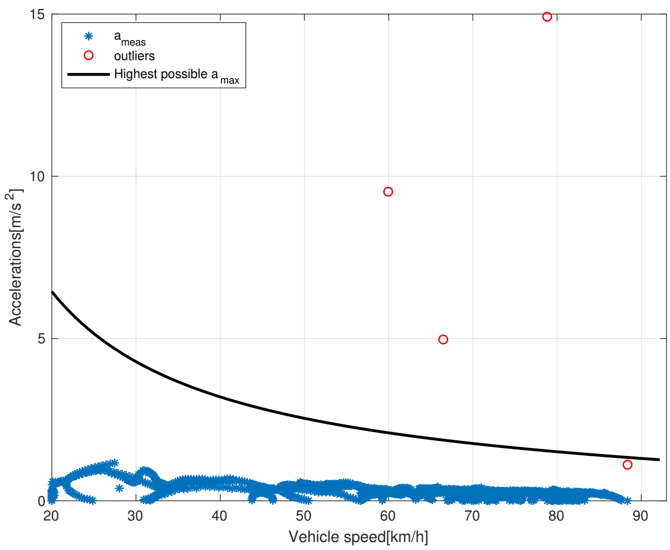

Figure 3.5: Acceleration a_{meas} after using the noise reduction approach.

3.6.3 Leading vehicle reference speed predictor

After the vehicle parameters l_0, l_1 and l_2 are obtained from the observer, they can then be used to determine if its desired speed $\bar{v}_{\mathrm{L}}$ (assumed to be known) is feasible or not. The speed trajectory of the leading vehicle, denoted by v_{Lr}, can then be predicted by numerically solving

$$v_{\mathrm{Lr}}(s) = \min\left\{\bar{v}_{\mathrm{L}}, \int_{s_0}^{s_{\mathrm{f}}} \min\left\{\frac{a_{\mathrm{com}}}{v_{\mathrm{Lr}}(s)}, \frac{a_{\mathrm{wLmax}}(s)}{v_{\mathrm{Lr}}(s)}\right\} ds\right\} \tag{3.31}$$

with initial value $v_{\mathrm{Lr}}(s_0)$ as the current speed of the leading vehicle. For comfort, a limit for how much the vehicle can accelerate for comfortable driving is also introduced, which is denoted by a_{com}. For those instances where $\bar{v}_{\mathrm{L}}$ is not considered feasible, the leading vehicle will drive with either a_{com} or maximum vehicle acceleration, denoted by a_{wLmax}, which is described by

$$a_{\mathrm{wLmax}}(s) = a_{\mathrm{max}} - g \cdot (\sin(\alpha) + c_{\mathrm{r}}\cos(\alpha)) \tag{3.32}$$

With the predicted speed trajectory, the traveling time of leading vehicle, denoted by t_{L}, can be calculated which will be used for the safety constraint described by Equation (2.29). The safety constraint will also be taken into account for prediction of speed trajectory of the host vehicle.

3.6.4 Host vehicle reference speed predictor

Prediction of speed trajectory of the host vehicle is similar to the case for the leading vehicle as described by Equation (3.31). For the host vehicle however, the safety constraint with t_{L} is also taken into consideration. Therefore, the prediction of the reference speed trajectory of the host vehicle, v_{r}, is calculated by

$$v_{\mathrm{r}}(s) = \min\left\{\bar{v}, v_{\mathrm{safe}}(s), \int_{s_0}^{s_{\mathrm{f}}} \min\left\{\frac{a_{\mathrm{com}}}{v_{\mathrm{r}}(s)}, \frac{a_{\mathrm{wmax}}(s)}{v_{\mathrm{r}}(s)}\right\} ds\right\} \tag{3.33}$$

where the initial value $v_{\mathrm{r}}(s_0 = 0) = \bar{v}$ and for the upcoming updates $v_{\mathrm{r}}(s_0 > 0) = v_0$ (current speed of host vehicle). The highest allowed speed of host vehicle based on the safety constraint, which is denoted by $v_{\mathrm{safe}}(s)$, is calculated by

$$v_{\mathrm{safe}}(s) = \frac{ds}{t_{\mathrm{L}}(s+1) - t_{\mathrm{L}}(s)} \tag{3.34}$$

where ds is the sample distance. The maximum acceleration of host vehicle, denoted by a_{wmax}, is described by

$$a_{\mathrm{wmax}}(s) = \frac{F_0}{m} + \frac{P_{\mathrm{Emax}}}{mv_{\mathrm{r}}(s)} - \frac{c_{\mathrm{a}}v_r^2(s)}{2m} - g(\sin(\alpha) + c_{\mathrm{r}}\cos(\alpha)) \tag{3.35}$$

The reference speed trajectory v_{r} is then sent to the energy management where the optimal state trajectories, including v, will be estimated.

3.7 Energy management

After variable change has been made as described in Section 3.4, the optimization problem has turned convex and can finally be solved in energy management. In this layer, the problem is reformulated as

$$\begin{aligned} &\text{minimize} \quad \tilde{J} = \int_{s_0}^{s_{\mathrm{f}}} (\chi(s)\tilde{\mu})ds \\ &\text{subject to} \end{aligned} \tag{3.36a}$$

$$t'(s) = f_t^{\mathrm{lin}}(E_{\mathrm{v}}(s)) \tag{3.36b}$$

$$\begin{aligned} E'_{\mathrm{v}}(s) =& \chi(s)F_{\mathrm{E1}}(s) + F_{\mathrm{E2}}(s) + F_{\mathrm{M}}(s) + F_{\mathrm{brk}}(s) + \chi(s)F_{\mathrm{Ebrk}}(s) + \\ &+ F_{\mathrm{air}}^{\mathrm{lin}}(E_{\mathrm{v}}, d_{\mathrm{LH}}) - mg(\sin(\alpha) + c_r\cos(\alpha)) \end{aligned} \tag{3.36c}$$

$$E'_{\mathrm{B}}(s) = -F_{\mathrm{B}}(s) \tag{3.36d}$$

$$F_{\mathrm{B}}(s) \geq \max\left\{\frac{F_{\mathrm{M}}(s)}{\eta}, \eta F_{\mathrm{M}}(s)\right\} + F_{\mathrm{Md}}(s) + F_{\mathrm{Bd}}(s) \tag{3.36e}$$

$$t(s_{\mathrm{f}}) \leq t_{\mathrm{max}} \tag{3.36f}$$

$$t(s_0) = t_0, \quad E_{\mathrm{v}}(s_0) = \frac{mv_0^2}{2} \tag{3.36g}$$

$$t(s) \geq t_{\mathrm{L}}(s) + \Delta t \tag{3.36h}$$

$$E_{\mathrm{v}}(s) \in \frac{m}{2}\left[v_{\mathrm{min}}^2(s), v_{\mathrm{max}}^2(s)\right] \tag{3.36i}$$

$$\chi(s)F_{\mathrm{E1}}(s) + F_{\mathrm{E2}}(s) \leq \eta P_{\mathrm{Emax}} f_t^{\mathrm{lin}}(E_{\mathrm{v}}(s)) \tag{3.36j}$$

$$F_{\mathrm{E1}}(s) \in \eta r(\gamma)\left[0, \min\left\{b_0, b_1 + \frac{2b_2r^2(\gamma)}{m}E_{\mathrm{v}}(s)\right\}\right] \tag{3.36k}$$

$$F_{\mathrm{Ebrk}} \in \left[\left(c_1 + \frac{2c_2}{m}E_{\mathrm{v}}(s)r^2(\gamma)\right), 0\right]\frac{r(\gamma)}{\eta} \tag{3.36l}$$

$$F_{\mathrm{brk}}(s) \leq 0, \quad F_{\mathrm{E2}}(s) \geq 0 \tag{3.36m}$$

$$F_{\mathrm{M}}(s) \in \left[F_{\mathrm{Mmin}}(E_{\mathrm{v}}), F_{\mathrm{Mmax}}(E_{\mathrm{v}})\right] \tag{3.36n}$$

$$E_{\mathrm{B}}(s_0) = E_{\mathrm{B0}}, \quad E_{\mathrm{B}}(s_{\mathrm{f}}) \geq E_{\mathrm{Bf}} \tag{3.36o}$$

$$E_{\mathrm{B}}(s) \in \left[\mathrm{SOC}_{\mathrm{min}}, \mathrm{SOC}_{\mathrm{max}}\right]E_{\mathrm{Bmax}} \tag{3.36p}$$

There are three states t, E_{v} and E_{B}, and six control signals F_{E1}, F_{E2}, F_{M}, F_{B}, F_{brk} and F_{Ebrk}. Note that integer states, such as γ and χ, as well as the penalty terms in Equation (3.2a) have been removed in this layer. There are several options for solving this convex problem. In this project, the problem is solved by quadratic programming [24].

After the optimization problem has been solved, the estimated trajectories for the speed v and battery costate λ_{B} are then sent to the power management. The control trajectories are also sent to obtain the demanded force F_{D} (more on this in Section 3.8.1).

3.8 Power management

Since power management has received the battery costate and optimal speed trajectory, constraints for v and travel time t in the optimization problem can be removed. The problem is thus reformulated as

$$\begin{aligned} &\text{minimize} \quad J = \int_{s_0}^{s_{\mathrm{f}}} (\chi\mu(F_{\mathrm{E}}, \gamma) + Q_{\mathrm{tot}}) ds \\ &\text{subject to} \end{aligned} \tag{3.37a}$$

$$E'_{\mathrm{B}}(F_{\mathrm{M}}, \gamma) = -F_{\mathrm{B}}(F_{\mathrm{M}}, \gamma) \tag{3.37b}$$

$$F_{\mathrm{D}}(s) = \chi(s)(F_{\mathrm{E1}}(s) + F_{\mathrm{Ebrk}}(s)) + F_{\mathrm{E2}}(s) + F_{\mathrm{brk}}(s) + F_{\mathrm{M}}(s) \tag{3.37c}$$

$$P_{\mathrm{B}}(F_{\mathrm{M}}, \gamma) = \max\left\{\frac{F_{\mathrm{M}}(s)}{\eta}, \eta F_{\mathrm{M}}(s)\right\} v(s) + P_{\mathrm{Md}}(\gamma, F_{\mathrm{M}}) + P_{\mathrm{Bd}}(P_{\mathrm{B}}) \tag{3.37d}$$

$$\chi(s)F_{\mathrm{E1}}(s) + F_{\mathrm{E2}}(s) \leq \frac{\eta P_{\mathrm{Emax}}}{v(s)} \tag{3.37e}$$

$$F_{\mathrm{E1}}(s) \in \left[0, \min\left\{b_0, b_1 + b_2 r^2(\gamma) v^2(s)\right\}\right] r(\gamma)\eta \tag{3.37f}$$

$$F_{\mathrm{Ebrk}}(s) \in \left[\left(c_1 + c_2 v(s)^2 r(\gamma)^2\right), 0\right] \frac{r(\gamma)}{\eta} \tag{3.37g}$$

$$F_{\mathrm{brk}}(s) \leq 0, \quad F_{\mathrm{E2}}(s) \geq 0 \tag{3.37h}$$

$$F_{\mathrm{Mmax}}(s) = \min\left\{d_1, d_2 + \frac{d_3}{v(s)r(\gamma)}\right\} r(\gamma)\eta \tag{3.37i}$$

$$F_{\mathrm{Mmin}}(s) = \max\left\{e_1, e_2 + \frac{e_3}{v(s)r(\gamma)}\right\} \frac{r(\gamma)}{\eta} \tag{3.37j}$$

$$E_{\mathrm{B}}(s_0) = E_{\mathrm{B0}}, \quad E_{\mathrm{B}}(s_{\mathrm{f}}) \geq E_{\mathrm{Bf}} \tag{3.37k}$$

$$E_{\mathrm{B}}(s) \in [\mathrm{SOC}_{\min}, \mathrm{SOC}_{\max}]\, E_{\mathrm{Bmax}} \tag{3.37l}$$

$$\chi^+(s) = \chi(s) + u_\chi(s), \quad \chi(s) \in X, \quad u_\chi(s) \in U_\chi \tag{3.37m}$$

$$\gamma^+(s) = \gamma(s) + u_\gamma(s), \quad \gamma(s) \in \Gamma, \quad u_\gamma(s) \in U_\gamma \tag{3.37n}$$

However, the demanded force F_{D} in (3.37c) has not been optimally divided between the forces, which will be done in power split. Note that the penalty term Q_{tot} has been introduced, which is described as

$$Q_{\mathrm{tot}} = W_\gamma(\gamma) + W_\chi(\chi) + F_{\mathrm{brk}}(s)^2 Q_{\mathrm{brk}} + F_{\mathrm{Ebrk}}(s)^2 Q_{\mathrm{ebrk}} + F_{\mathrm{E2}}(s) Q_{\mathrm{Fe2}} \tag{3.38}$$

where Q_{brk}, Q_{ebrk} and Q_{Fe2} are the penalties for applying F_{brk}, F_{Ebrk} and F_{E2}, respectively. As F_{E2} should be avoided, Q_{Fe2} is put relatively high compared to the other penalties. Since it is desirable to apply less F_{brk} than F_{Ebrk} for braking, Q_{brk} is put significantly higher than Q_{ebrk}.

The problem can be solved by first formulating a Hamiltonian which is expressed as

$$\mathcal{H}(F_{\mathrm{E}}, F_{\mathrm{B}}, \gamma, \chi) = \chi \tilde{\mu}(\gamma, F_{\mathrm{E}}) + Q_{\mathrm{tot}} - \lambda_{\mathrm{B}}(s) F_{\mathrm{B}}(\gamma, \chi, F_{\mathrm{M}}) \tag{3.39}$$

A necessary condition for optimality is described by

$$\left(\frac{\partial \mathcal{H}}{\partial E_{\mathrm{B}}}\right)^* - \frac{d}{ds}\left(\frac{\partial \mathcal{H}}{\partial E'_{\mathrm{B}}}\right)^* = 0 \implies \lambda'_{\mathrm{B}}(s) = 0 \tag{3.40}$$

This means that λ_{B} should be constant over traveled distance for each predicted horizon, provided that E_{B} does not hit its limits, though it is likely to happen in real scenario. However, for this project it is assumed that the battery is large enough to avoid hitting the limits. Since λ_{B} should penalize the usage of EM as indicated in Equation (3.39), it should also be negative.

3.8.1 Power split

When power split is performed, the gear γ and ICE-state χ have already been given (later described in Section 3.8.2). For simplicity, instance s has also been omitted in this section. A set of feasible F_{M}-points (including F_{Mmin} and F_{Mmax}), which is denoted by F_{Mfeas}, is first created

$$F_{\mathrm{Mfeas}} \in \{F_1, F_2, ..., F_{\mathrm{G}}\} \tag{3.41}$$

where G is the number of feasible F_{M}-points. If F_{D} also lies within the limits of F_{M}, then it also included in F_{Mfeas}.

The battery force F_{B}, as function of F_{Mfeas}, needs to be expressed by using following Equations

$$P_{\mathrm{M}}(F_{\mathrm{Mfeas}}) = \omega_{\mathrm{M}} r F_{\mathrm{Mfeas}} \tag{3.42}$$

$$P_{\mathrm{Md}}(F_{\mathrm{Mfeas}}) = h_1\omega_{\mathrm{M}} + h_2\omega_{\mathrm{M}}^3 + h_3\omega_{\mathrm{M}} r \left|\max\left\{\frac{F_{\mathrm{Mfeas}}}{\eta}, \eta F_{\mathrm{Mfeas}}\right\}\right| \tag{3.43}$$

$$P_{\mathrm{Bd}}(P_{\mathrm{B}}) = \frac{R}{V_{\mathrm{oc}}^2} P_{\mathrm{B}}^2 \tag{3.44}$$

$$P_{\mathrm{B}} = P_{\mathrm{M}} + P_{\mathrm{Md}}(F_{\mathrm{Mfeas}}) + P_{\mathrm{Bd}}(P_{\mathrm{B}}) = P_{\mathrm{M}} + P_{\mathrm{Md}}(F_{\mathrm{Mfeas}}) + \frac{R}{V_{\mathrm{oc}}^2} P_{\mathrm{B}}^2 \tag{3.45}$$

By solving the quadratic Equation (3.45) for P_{B}, it can be expressed as

$$P_{\mathrm{B}}(F_{\mathrm{Mfeas}}) = \frac{V_{\mathrm{oc}}^2}{2R} - \sqrt{\left(\frac{V_{\mathrm{oc}}^2}{2R^2}\right)^2 - \frac{V_{\mathrm{oc}}^2}{R}(P_{\mathrm{Md}}(F_{\mathrm{Mfeas}}) + P_{\mathrm{M}}(F_{\mathrm{Mfeas}}))} \tag{3.46}$$

which is then used to express F_{B} as

$$F_{\mathrm{B}}(F_{\mathrm{Mfeas}}) = \frac{P_{\mathrm{B}}(F_{\mathrm{Mfeas}})}{v} \tag{3.47}$$

The rest of the control signals, as function of F_{Mfeas}, are calculated as

$$F_{\mathrm{E2}}(F_{\mathrm{Mfeas}}) = \max\{0, F_{\mathrm{D}} - F_{\mathrm{Mfeas}} - F_{\mathrm{Emax}}\} \tag{3.48a}$$

$$F_{\mathrm{E1}}(F_{\mathrm{Mfeas}}) = \max\{0, F_{\mathrm{D}} - F_{\mathrm{Mfeas}} - F_{\mathrm{E2}}(F_{\mathrm{Mfeas}})\} \tag{3.48b}$$

$$F_{\mathrm{brk}}(F_{\mathrm{Mfeas}}) = \min\{0, F_{\mathrm{D}} - F_{\mathrm{Mfeas}} - F_{\mathrm{ebrkmin}}\} \tag{3.48c}$$

$$F_{\mathrm{Ebrk}}(F_{\mathrm{Mfeas}}) = \min\{0, F_{\mathrm{D}} - F_{\mathrm{Mfeas}} - F_{\mathrm{brk}}(F_{\mathrm{Mfeas}})\} \tag{3.48d}$$

The limits for the force delivered by ICE in (3.48) are described by

$$F_{\mathrm{Emax}} = \min\left\{\frac{\eta P_{\mathrm{Emax}}}{v}, b_0 r(\gamma)\eta, (b_1 + b_2 r^2(\gamma)v^2) r(\gamma)\eta\right\} \tag{3.49a}$$

$$F_{\mathrm{ebrkmin}} = (c_1 + c_2 v^2 r(\gamma)^2)\frac{r(\gamma)}{\eta} \tag{3.49b}$$

The point from F_{Mfeas} which gives the least value of Hamiltonian in Equation (3.39) becomes the optimal F_{M}, which can then be used to obtain the rest of the optimal control trajectories. However, the gear and ICE-state trajectories have not been determined, which is done by dynamic programming [25].

3.8.2 Dynamic Programming

The states of DP (Dynamic Programming) are the gears and ICE-state, which can be expressed as $\zeta(s) = [\gamma, \chi]$. It first performs backward optimization where the initial instance is $s = s_\mathrm{f} - 1$ and then moves backward to reach next instance. For every instance that has been reached and for every state, the optimization calculates the minimum but feasible cost

$$J(\zeta(s), s) = \min_{\zeta(s+1) \in \zeta_\mathrm{feas}} \{C(\zeta(s), \zeta(s+1), s) + J(\zeta(s+1), s+1)\} \tag{3.50}$$

where $\zeta_\mathrm{feas} = [\Gamma_\mathrm{feas}, X_\mathrm{feas}]$ are feasible updates of states at $s+1$ and $C(\zeta(s))$ is the cost for being at the state at instance s.
The feasible state updates that can be reached at instance $s{+}1$ are expressed as

$$\Gamma_\mathrm{feas} = \Gamma \cap (\gamma(s) + U_\gamma), X_\mathrm{feas} = X \cap (\chi(s) + U_\chi) \tag{3.51}$$

In the Hamiltonian cost (3.39), the penalties W_γ and W_χ have the weights w_γ and w_χ, respectively. They are added based on the decision variables y_γ and y_χ, which are described by

$$y_\gamma(\gamma(s), \gamma(s+1)) = \begin{cases} 1, & \text{if } \gamma(s+1) < \gamma(s) \\ 0, & \text{otherwise} \end{cases} \tag{3.52a}$$

$$y_\chi(\chi(s), \chi(s+1)) = \begin{cases} 1, & \text{if } \chi(s+1) \neq \chi(s) \\ 0, & \text{otherwise} \end{cases} \tag{3.52b}$$

In other words, w_γ is added when the selected gear at one instance is higher than the selected gear at next instance due to downshift. The weight w_χ is added when the ICE-state is changed from one instance to the next. Both weights are tuned accordingly to avoid frequent shifts.

Once the backward optimization has reached $s = s_0$, the forward optimization begins. It then chooses the optimal path with minimum cost among the costs of all feasible paths. The optimal state at next instance can be expressed as

$$\zeta^*(s+1) = \arg\min_{\zeta(s+1) \in \zeta_\mathrm{feas}} \{C(\zeta^*(s), \zeta(s+1), s) + J(\zeta(s+1))\} \tag{3.53}$$

where $\zeta^*(s)$ is the optimal state at instance s.

3.8.3 Battery costate optimization

The battery costate trajectory λ_B, received from the energy management, is not optimal as there is model miss-match between the two layers. This might lead to that the final battery energy $E_{\mathrm{B}}(s_{\mathrm{f}})$ deviates significantly from its target E_{Bf}. Therefore, λ_{B} needs to be adjusted iteratively [11][26] such that the battery energy error ΔE_{Bf} satisfies

$$\Delta E_{\mathrm{Bf}} = E_{\mathrm{B}}(s_{\mathrm{f}}) - E_{\mathrm{Bf}} \approx 0 \tag{3.54}$$

Thus, for each iteration the dynamic programming needs to be run again to adjust λ_{B}. The adjustment is done by increasing/decreasing with a stepsize δ. For example if $\Delta E_{\mathrm{Bf}} < 0$, it means that too much EM-force has been applied and λ_{B} has to decrease ($\lambda_{\mathrm{B}} := \lambda_{\mathrm{B}} - \delta$) to penalize more and vice versa. If there has been a sign change of calculated ΔE_{Bf} between two iterations, then $E_{\mathrm{B}}(s_{\mathrm{f}})$ has passed E_{Bf}, and δ can be decreased with a factor to make better adjustments for next iterations. The battery energy $E_{\mathrm{B}}(s)$ can be obtained by integrating (3.37b) in space domain.

The procedure for updating λ_{B} is illustrated by the flow chart in Figure 3.6. It can be described by following pseudocode where c is the iteration for updating λ_{B}:

1. Calculate $\Delta E_{\mathrm{B}}^{c}(s_{\mathrm{f}})$ after running dynamic programming.
2. If $\Delta E_{\mathrm{B}}^{c}(s_{\mathrm{f}}) \leq$ bound, then finish. Else move to step 3.
3. $\lambda_{\mathrm{B}}^{c} = \lambda_{\mathrm{B}}^{c-1} + \mathrm{sign}(\Delta E_{\mathrm{Bf}}^{c})\delta$.
4. If $\mathrm{sign}(\Delta E_{\mathrm{Bf}}^{c}) = -\mathrm{sign}(\Delta E_{\mathrm{Bf}}^{c-1})$ move to step 5. Else move to step 6.
5. $\delta := \frac{\delta}{2}$
6. $c := c + 1$ and return to step 1.

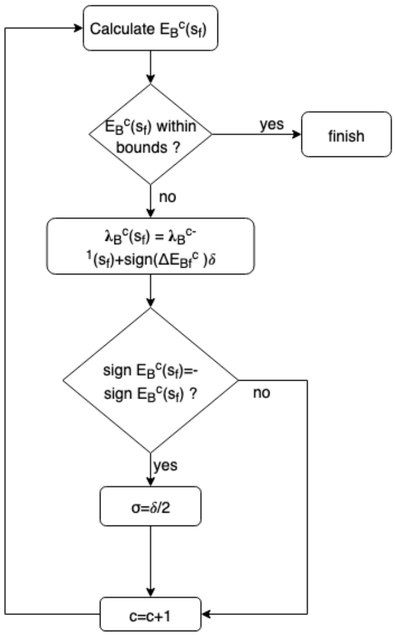

Figure 3.6: Flow chart of the battery co-state update. The number of update is denoted by c.

Both δ and c are reset to their initial values before the next MPC-update.

3.9 Summary of MPC-algorithm

A flowchart of the complete MPC-algorithm is shown in Figure 3.7, which can be summarized by following steps:

1. Starting from the beginning of the road where current instance $s_0 = 0$, the position of leading vehicle is located and a constant cruising speed $\bar{v}$ is set for the host vehicle.
2. At s_0, the host vehicle collects measurement data from the leading vehicle, including its travel time and speed. The data is then sent to the leading vehicle observer which estimates the parameters l_0,l_1 and l_2.
3. Based on the estimated parameters and an assumed cruising speed $\bar{v}_{\mathrm{L}}$, the leading vehicle reference speed predictor obtains the reference speed trajectory v_{Lr}. This trajectory is used to estimate the traveling time trajectory of leading vehicle t_{L}, which is then sent to both energy management and the host vehicle speed predictor. The host vehicle speed predictor uses information of t_{L} and road topography to obtain host vehicle reference speed trajectory v_{r} and send it to the energy management.
4. In the energy management, the optimization problem is solved which yields the optimal speed trajectory v and battery costate trajectory λ_{B}. Both trajectories are sent to the power management. In the first iteration, the highest gear is selected and ICE-state is on for all predicted instances.
5. The problem is solved in power management to find the optimal trajectories for control signals, gear and ICE-state. It is solved repeatedly, until λ_{B} has been updated such that $E_{\mathrm{B}}(s_{\mathrm{f}})$ lies within its bounds. The gear and ICE-state trajectories are then sent to energy management.
6. If the solution has not converged or a maximum number of iteration has not been reached, return to step 4. During each iteration, the reference speed trajectory v_{r} is updated as

   $$v_{\mathrm{r}} := v_{\mathrm{r}} + (v_{\mathrm{r}} + (v - v_{\mathrm{r}}))\beta \tag{3.55}$$

   where $\beta \in (0, 1]$ is a convergence step.
7. Apply the first element of the optimal control trajectories $\mathbf{U}(s_0{:}s_{\mathrm{f}})$ and discard the rest. If the final instance of the road, s_{N}, has been reached, finish the procedure. Otherwise, move to the next instance and return to step 2.

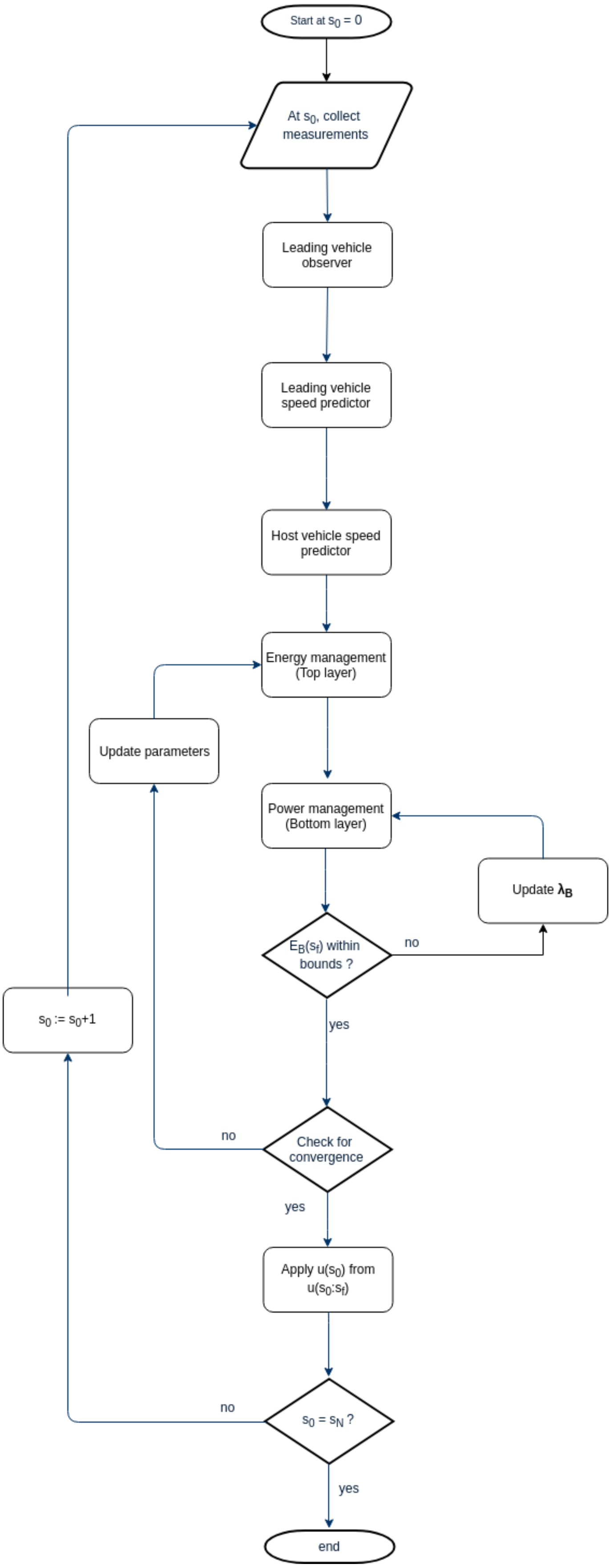

Figure 3.7: Flow chart of the implemented MPC-algorithm

4
Results

In this chapter, the results obtained in this project are presented. For the driving scenarios, two different road topographies are used:

1. An artificial driving cycle with a length of 7km as seen in Figure 4.1.
2. The second driving cycle is a road between Alingsås and Gothenburg as seen in Figure 4.2. This is primarily used for investigating different case scenarios which involve leading vehicle.

The investigations are done with host vehicle, both as CV and HEV. In Section 4.1, the host vehicle driving on the road displayed in Figure 4.1 is shown to see how it behaves without leading vehicle present. For the rest of the results, the driving cycle in Figure 4.2 is used which involves leading vehicle. With leading vehicle present, The length of predicted horizon is also examined. For all results, the sample distance is set as 100m for prediction.

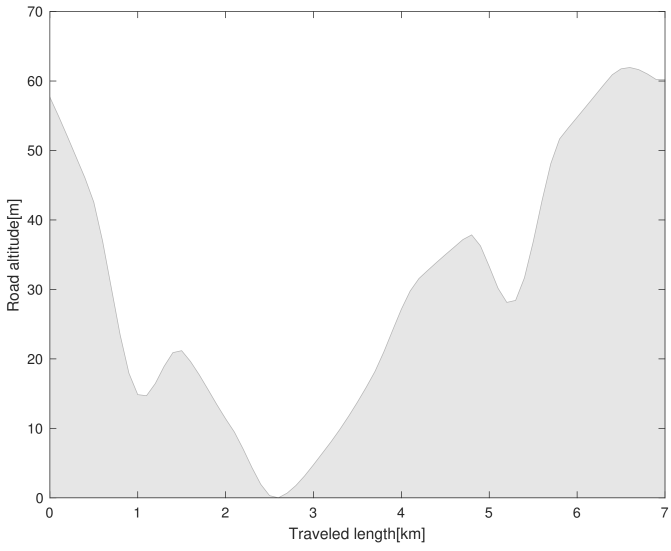

Figure 4.1: Artificial driving cycle with a road length of 7km. The horizontal axis represents the traveled distance and the vertical axis represents the altitude.

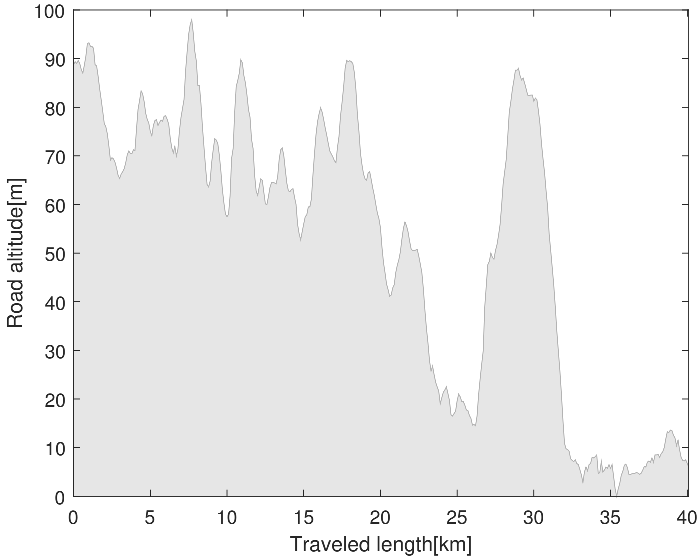

Figure 4.2: Road between Alingsås and Gothenburg. The length of the driving cycle is 40.1km.

4.1 Validation of control algorithm without LV

In this section, the control algorithm is validated both for CV and HEV without a leading vehicle present. Since there is no LV (Leading Vehicle) present, the prediction horizon is set as the entire road and MPC needs to be run for one update only. The cruising speed is set as $\bar{v} = 80$km/h. The speed tolerance is set as $\pm$ 10km/h, meaning that the speed can deviate at most 10km/h from the reference speed.

4.1.1 CV without LV ahead

In Figure 4.3, the optimal speed and gear trajectories are shown with the speed limits. There are some instances where the speed hits its limits, but it still remains in the feasible region during the entire travel. The lowest selected gear is nine and its trajectory does not downshift frequently.

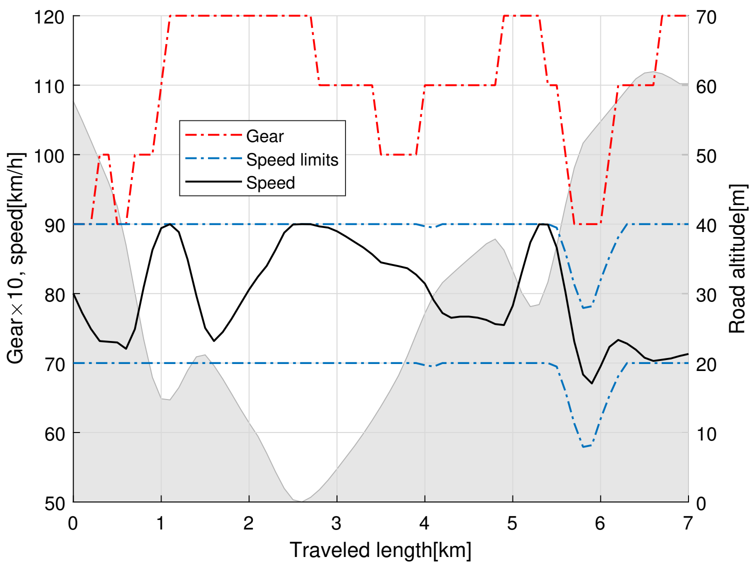

Figure 4.3: The state trajectories of CV and the speed limits. The ICE-state is not included since the engine is always on for CV.

The corresponding control trajectories to Figure 4.3 are depicted in Figure 4.4. In the beginning where there is a very steep downhill, large frictional force by the engine is applied such that it hits its limit. At one instance, the gear even needs to be downshifted to apply even more frictional engine force. When traveling uphill, the host vehicle starts applying engine force. Note that the engine force is never applied at the same time as either braking or frictional engine force is. The abstract force remains zero for the entire travel, so the gear trajectory has been properly selected.

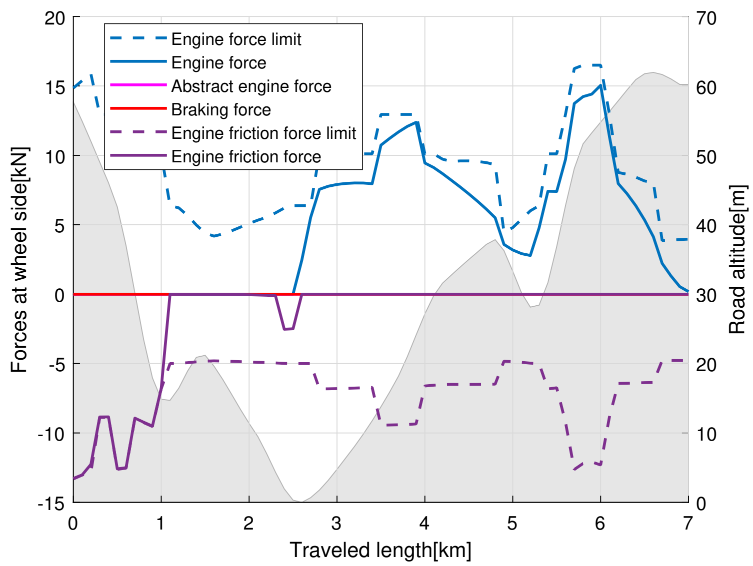

Figure 4.4: The control trajectories of CV and ICE limits. EM force and its limits are not displayed since they are not available for CV.

4.1.2 HEV without LV ahead

In this case, EM force and SOC (the battery charge in percentage) are available. The initial battery energy is assumed to be $E_{\mathrm{B0}} = 0.6E_{\mathrm{Bmax}}$ and the targeted final battery energy is chosen as $E_{\mathrm{Bf}} \approx 0.4E_{\mathrm{Bmax}}$. Figure 4.5 displays the state trajectories of HEV, including its ICE-state and SOC, and Figure 4.6 displays the control trajectories.

Compared to CV, HEV maintains higher gear trajectory as it is able to utilize force from EM. Similar to the speed trajectory of CV, there are some instances where the speed hits its limits but also remains within its feasible region. SOC increases when EM works as generator (negative EM force applied) and decreases when EM works as motor (positive EM force applied). However, SOC never hits its limits for the entire travel.

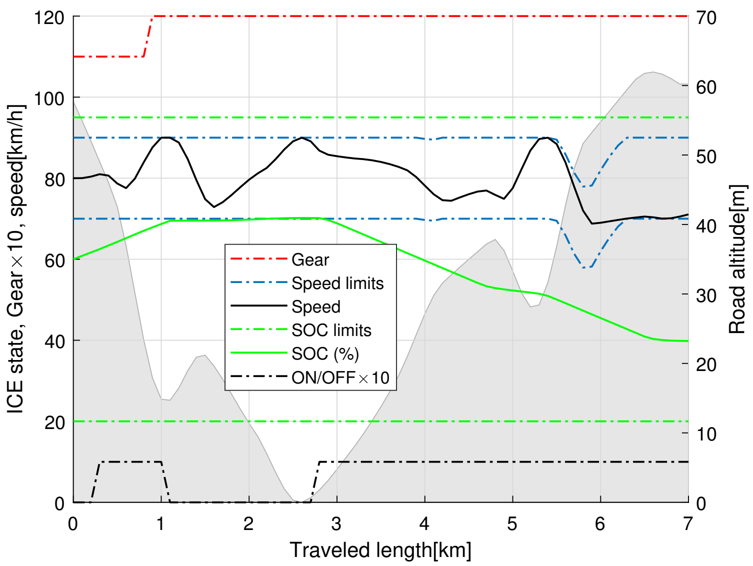

Figure 4.5: The state trajectories of HEV, including ICE-state and SOC, as function of traveled distance. The limits for SOC and speed are also displayed.

In the beginning, ICE is off and only negative EM force is applied. However, since EM force reaches its limit later and more braking is required, an amount of frictional force by the engine is applied as well and ICE has to be turned on. Positive EM force is applied when HEV travels uphill, so that less engine force is needed for propulsion. Note that in the interval 1-2.7km, where neither of the forces from engine is applied, ICE is turned off again. EM force hits its upper limit at numerous instances.

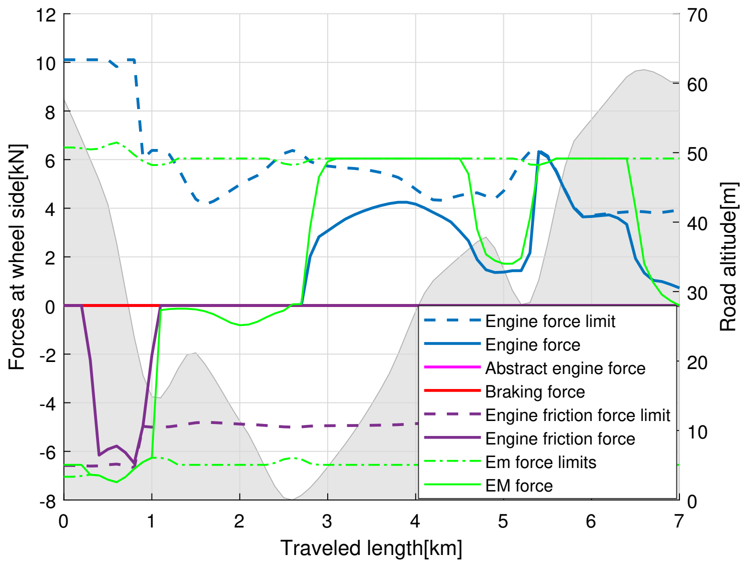

Figure 4.6: The control trajectories of HEV, including EM force, as function of traveled distance. The limits for ICE and EM are also displayed.

4.2 Validation of control algorithm with LV

In this section, the control algorithm is evaluated when there is a leading vehicle driving in front of host vehicle. Therefore, the leading vehicle observer has to be used to estimate its power capability. Real measurement data of a leading vehicle driving on the road topography in Figure 4.2 is used.

The leading vehicle is assumed to have been detected at 200m from the start of the road. Therefore, a new MPC-update is made for each instance that host vehicle reaches. Since it is unknown of what the desired speed of leading vehicle $\bar{v}_{\mathrm{L}}$ is, it is set as the average value of the collected measured speed between updates or as minimum 60km/h. The length of prediction horizon is set as Sp=4km and the desired speed of host vehicle is set as $\bar{v}$ =90km/h. For the safety constraint, the time headway is set as Δt =2s.

4.2.1 LV observer

Figure 4.7 shows the performance of observer dependent on the traveled distance of leading vehicle along with its actual acceleration limit. The further leading vehicle travels, the more measurements are collected. A sample distance of 5m is used to collect the measurement data. The number of speed clusters is chosen as 10.

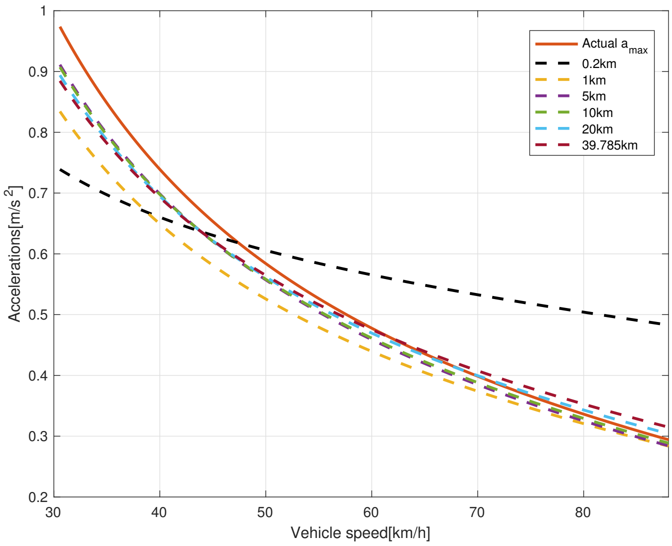

Figure 4.7: The various estimated acceleration limits as function of vehicle speed. The estimation of limits depend on the traveled distance of leading vehicle.

All estimated limits are non-concave due to the boundaries put for the parameters. The limit that is obtained after leading vehicle has driven only for 200m is the one that deviates most from the actual limit, as there is not enough measured points collected to make a proper estimation. However, after the leading vehicle has driven further, more measurement data is collected and the observer makes better estimation of the limit. The various estimated accelerations limits obtained after leading vehicle has driven 1km and further are closer to the actual limit compared to the one when the leading vehicle has only driven for 200m.

4.2.2 CV with LV ahead

The state trajectories, which include gear and speed, are seen in Figure 4.8. Since the desired speed $\bar{v}$ is now set higher than in Section 4.1 and the speed needs to be adjusted to not get too close to leading vehicle, the speed limits vary a lot more. The speed hits the limits at some instances, but remains within its feasible region during the entire travel.

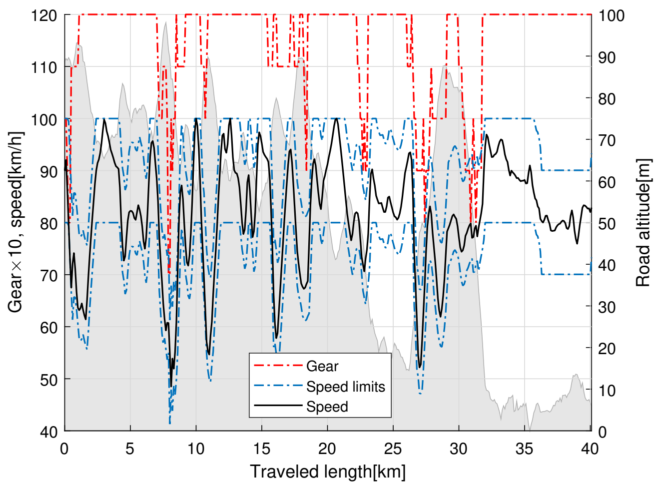

Figure 4.8: The state trajectories of CV as function of traveled distance and the speed limits.

The control trajectories of host vehicle is seen in Figure 4.9. Note that at instance 7.9km where there is a very steep downhill, the gear has to be downshifted to a much lower level to be able to apply much larger frictional force by the engine. For uphills, the engine force is applied. Neither abstract force nor mechanical braking force (braking force by the service brake) is applied for the entire travel.

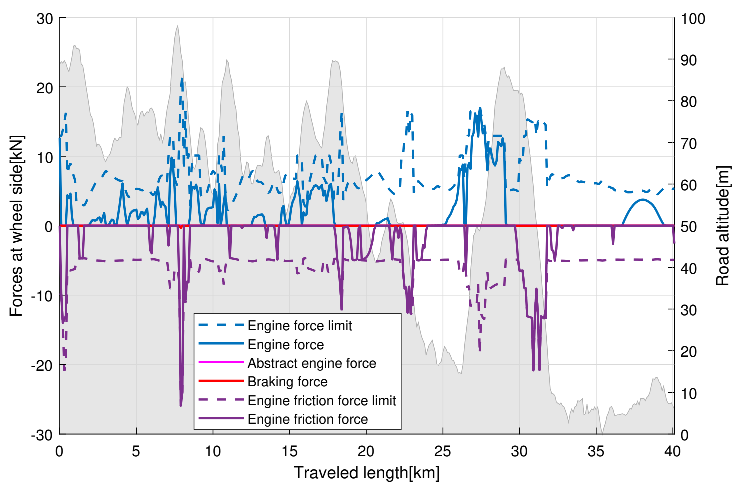

Figure 4.9: The control trajectories of CV as function of traveled distance and the ICE limits.

Figure 4.10 shows the gap between the traveling times of host and leading vehicle. There are some instances where the gap goes a little bit below the time headway. However, the most important thing is that it never goes to 0, meaning that host vehicle never collides with leading vehicle. Note that gap is biggest at around 32.5km. This could be that the calculated desired speed of leading vehicle is significantly lower than the actual desired speed, which makes the gap bigger as host vehicle drives slower.

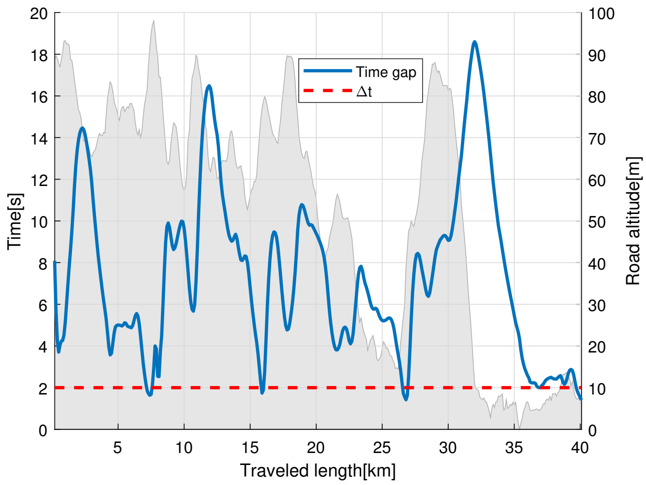

Figure 4.10: The time gap between the traveling times of leading vehicle and host vehicle (CV) as function of traveled distance.

4.2.3 HEV with LV ahead

In the beginning of the road, the battery energy is assumed to be $E_{\mathrm{B0}} = 0.6E_{\mathrm{Bmax}}$. For simplicity, λ_{B} should be updated such that the targeted battery energy becomes $E_{\mathrm{Bf}} \approx 0.6E_{\mathrm{Bmax}}$ by the end of horizon.

Figure 4.11 shows the state trajectories of host vehicle as HEV. Compared to Figure 4.8, the gear trajectory is higher. The lowest selected gear is 10, but the trajectory remains on gear 12 during most of the travel. SOC varies during travel, but never hits its limits. Except for the instances around 28-29km and in the beginning of the road, the ICE-state does not shift frequently between the updates.

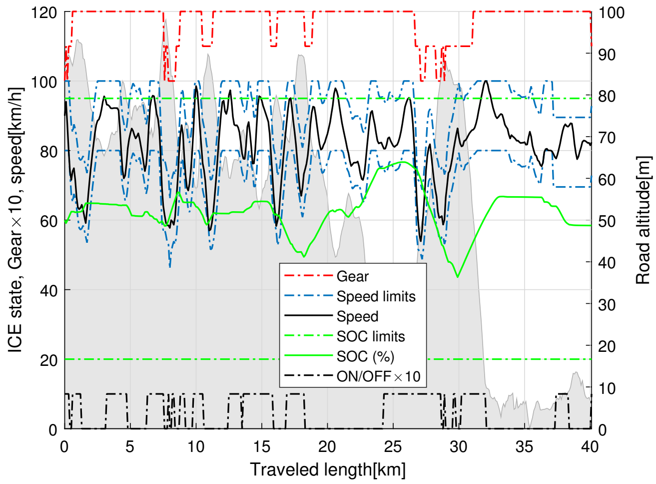

Figure 4.11: The state trajectories of HEV as function of traveled distance. The limits for SOC and speed are also displayed.

Figure 4.12 illustrates the control trajectories and their limits. Positive EM force is applied when going uphill and sometimes requires ICE to be turned on to apply engine force as well. There are some instances where negative EM force and engine force are applied at the same time, which is sometimes needed to charge the battery. When traveling downhill, negative EM force is applied to brake and generate energy to the battery. However, since there are some instances where the downhill is very steep, ICE still needs to be turned on to apply frictional engine force as EM force has already reached its limit. Since the abstract force is never applied during the entire travel, the gear trajectory has been properly selected.

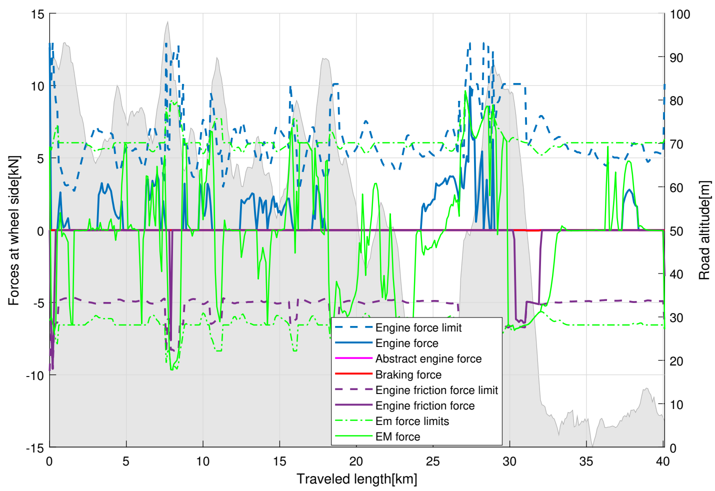

Figure 4.12: The control trajectories of HEV as function of traveled distance. The limits for ICE and EM are also displayed.

The time gap is illustrated in Figure 4.13. It is shown in the Figure that the host vehicle maintains a safe distance to the leading vehicle throughout the driving cycle. There are a few instances where the gap goes a little bit below Δt, but it never gets close to 0. This means that host vehicle never gets too close or collides with leading vehicle in front.

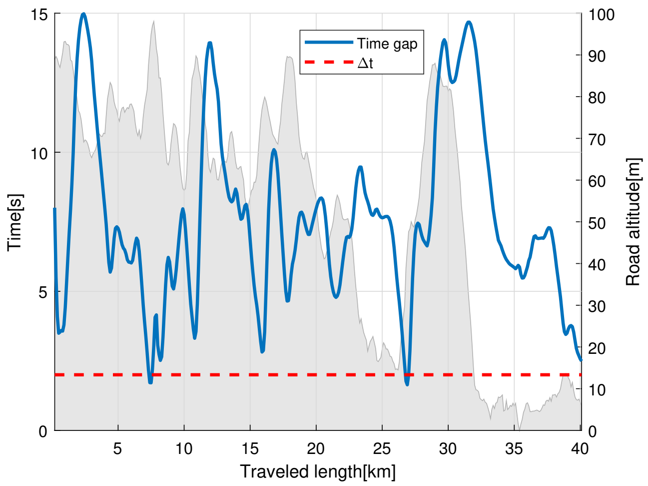

Figure 4.13: The time gap between the traveling times of leading vehicle and host vehicle (HEV) as function of traveled distance.

By comparing the results of CV and HEV in Figures 4.8 and 4.11, it is shown that HEV does not need to downshift the gear as frequently as CV. This is because EM supports ICE for delivering demanded force. In Figures 4.9 and 4.12, it can be seen that the HEV applies less frictional force by the engine as it is able to use EM for braking. By using EM for braking, the HEV also recovers energy and stores it in the battery, which is later used for propulsion.

4.3 Length of prediction horizon

In this section, the length of prediction horizon is examined to see how it affects the performance of the control algorithm. Same driving scenario with similar settings as described in Section 4.2 are used here.

Table 4.1 shows the fuel consumption and final traveling time of host vehicle as CV for other selected lengths of prediction horizon. It also includes t_{sum}, which is the sum of the time gap going below Δt. In other words, t_{sum} shows how much the safety constraint has been violated during the entire travel. For the case when the prediction horizon is set as the entire road length, MPC is run for one update only.

Table 4.1: Fuel consumption, final traveling time and t_{sum} of CV for different prediction horizon.

S_{p}[km]	Fuel[kg]	t_{f}[min]	t_{sum}[s]
Entire road length	6.9163	39.953	0
1	7.7115	30.0816	10.09
2	5.9472	30.0758	5.43
3	5.9576	30.0814	4.05
4	5.402	30.0727	4.83

For the shorter prediction horizons (1-4km), it can be seen that the highest fuel consumption is for the case with Sp=1km and lowest for the case with Sp=4km. Normally, what is expected is that the fuel consumption will monotonically decrease the longer prediction horizon is as more instances of the road topography ahead are taken into consideration. However, the fuel consumption for the case with Sp=3km is slightly higher compared to the one for the case with Sp=2km. It is shown that the host vehicle travels faster and also uses more engine braking in the case with Sp=3km than Sp=2km. This is likely because of uncertainty of the leading vehicle speed prediction at some instances for Sp=3km. For some MPC-updates, the host vehicle predicts that the leading vehicle will travel faster, but then it predicts that the leading vehicle travel will travel significantly slower in the next update. Therefore, the host vehicle drives faster first but then it has to apply more engine brake as it predicts the leading vehicle will drive significantly slower in the next update. Thus, fuel consumption, which is the function of speed and engine force as shown in Equation (2.9), is higher for the case with Sp=3km.

A similar table for HEV is shown in Table 4.2. The initial battery energy E_{B0} and targeted final battery E_{Bf} have been set the same as in Section 4.2.3, regardless of length of prediction horizon.

Table 4.2: Fuel consumption, final traveling time and t_{sum} of HEV for different lengths of prediction horizon.

S_{p}[km]	Fuel[kg]	t_{f}[min]	t_{sum}[s]
Entire road length	1.3408	39.953	0
1	3.5025	30.0824	8.48
2	3.26	30.0728	3.80
3	2.8474	30.0807	0.44
4	2.3425	30.0907	1.1825

With HEV, the fuel consumption decreases the longer horizon that is selected as more instances of the road topography are taken into consideration.

Note that for both CV and HEV, t_{sum} is 0 but the final traveling time is much longer when the prediction horizon is set as the entire length and run for one update only. This can be explained by Figure 4.14 which shows a comparison between the predicted and actual speed of leading vehicle and its constant desired speed which has been assumed to be 60km/h. Since the leading vehicle has been detected at 200m from the beginning of the road, the observer has estimated its acceleration limit as the one shown in Figure 4.7 after it has driven 0.2km. With the acceleration limit, the speed leading vehicle been predicted to maintain its assumed desired speed for the entire road.

However, except for the instance around 8km, the predicted speed is considerably lower than the actual one for the entire travel. This means that host vehicle believes that the leading vehicle drives significantly slower than it actually does, which leads to the host vehicle also drives slower. Therefore, the safety constraint is never violated, but the time gap between the vehicles increases over traveled distance and the final travel time of host vehicle is longer compared to the cases with shorter prediction horizons.

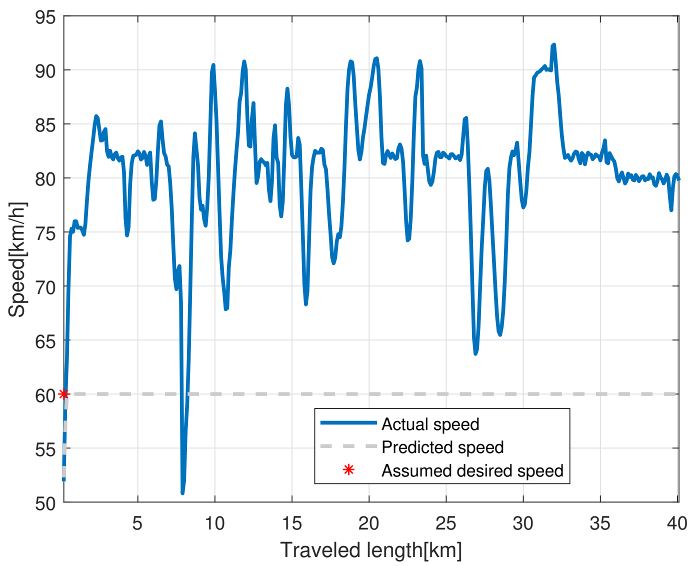

Figure 4.14: The actual and predicted speed of leading vehicle and its assumed desired speed when the prediction is done once for the entire road.

Figures 4.15 and 4.16 show the time gaps for different lengths of prediction horizon as function of traveled distance for CV and HEV, respectively. As the results of t_{sum} in Tables 4.1 and 4.2 indicate, the safety constraint has been violated for the shorter prediction horizons. But most importantly, neither of them gets close to or below 0. For both CV and HEV, the safety constraint is never violated for the case where prediction horizon is set as the entire road length, but the gap increases over traveled distance.

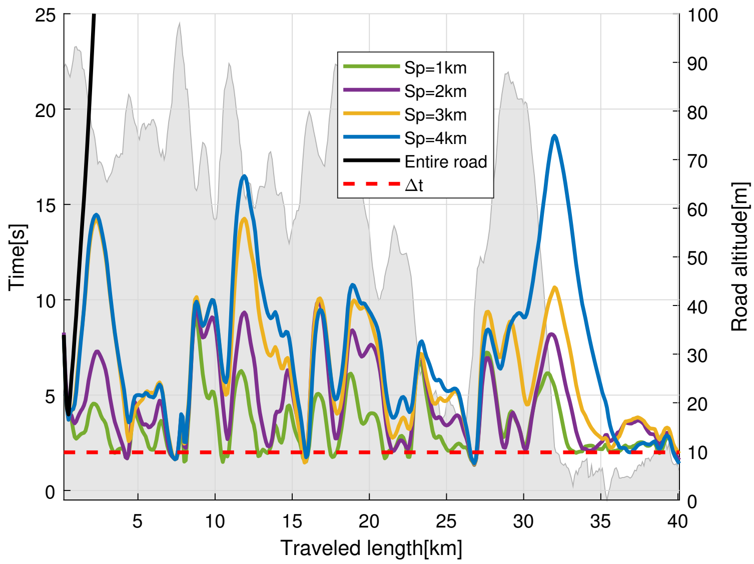

Figure 4.15: Time gaps for different lengths of prediction horizon as function of traveled distance for CV. Note that the rest of the gap represented by the black line is not displayed as it increases significantly over traveled distance.

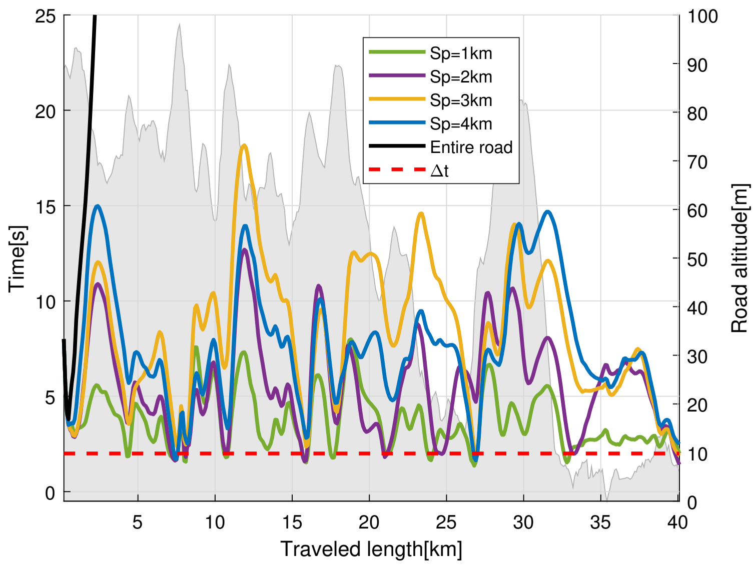

Figure 4.16: Time gaps for different lengths of prediction horizon as function of traveled distance for HEV.

4.4 No observer available

In this section, similar case scenario as described in Section 4.2 is examined when the observer is not available. Only HEV as host vehicle is considered and the same settings described in Section 4.2.3 are used. This case is important to study the benefit of the observer when comparing with the results in Section 4.2.3.

For each MPC-update, only the current speed of leading vehicle is measured and the host vehicle assumes it to be constant over the predicted horizon. If the current speed of leading vehicle is less than 60km/h, the host vehicle assumes that leading vehicle will maintain a constant speed of 60km/h.

The control trajectories are seen in Figure 4.17. Compared to Figure 4.12, a significantly larger frictional force by engine is applied along with force by service brake at around 8km in this case. This is because the host vehicle can only assume that leading vehicle will maintain its current speed over predicted horizon. In the next MPC-update however, the current speed of leading vehicle is measured to be lower and host vehicle needs to slow down significantly by applying more braking force.

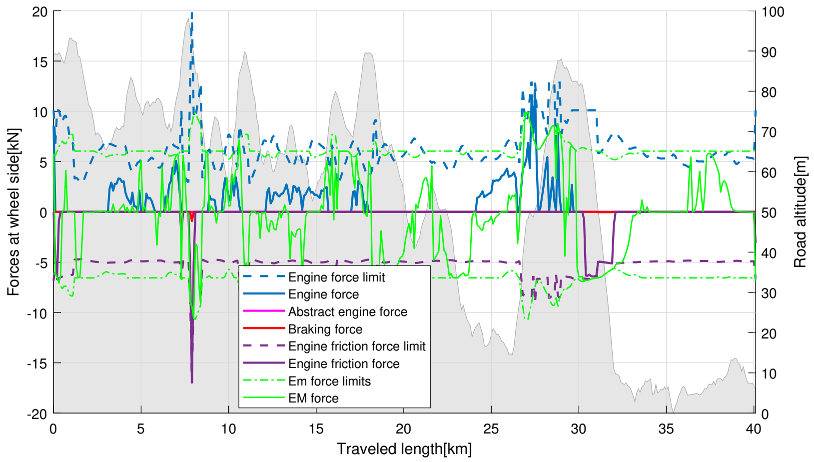

Figure 4.17: The control trajectories as function of traveled distance when the observer is not available.

The time gap between host and leading vehicle is shown in Figure 4.18. There are some instances where the gap goes below Δt, but it never reaches 0. However, compared to Figure 4.13, the safety constraint is more violated in this case.

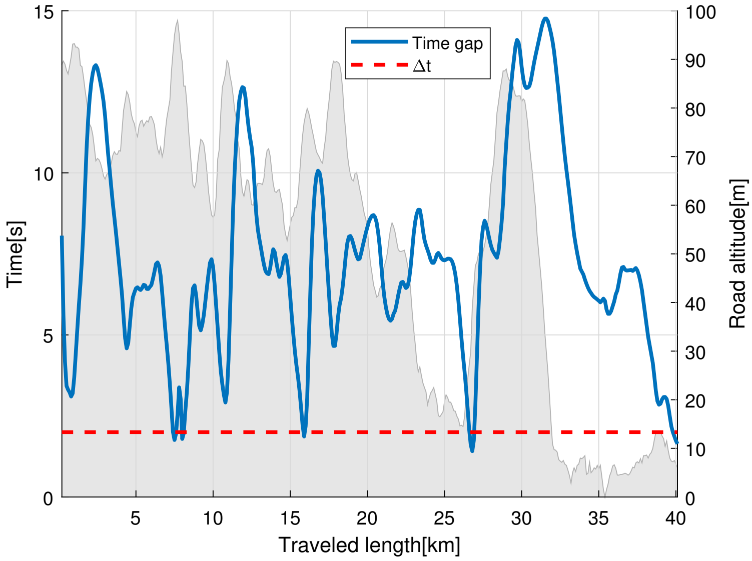

Figure 4.18: The time gap as function of traveled distance when the observer is not available.

Figure 4.19 shows the predicted speed trajectories of leading vehicle along with its actual speed trajectory. The assumed desired speed for each sample is also shown. As the current speed of leading vehicle is assumed to be constant over predicted horizon for each update, the predicted speed trajectories deviate significantly from the actual trajectory.

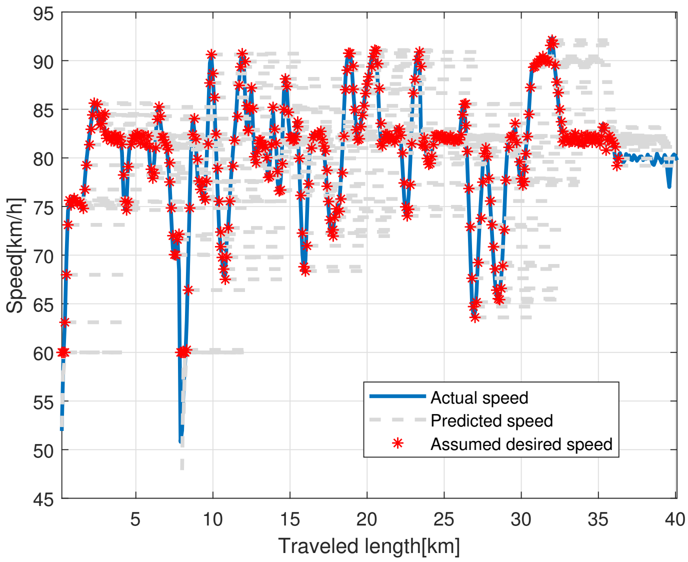

Figure 4.19: The predicted speed trajectory and the assumed desired speed of the leading vehicle for each sample along with the actual speed trajectory when observer is not available.

Note that for those updates where the current speed is lower than 60km/h, the host vehicle assumes that leading vehicle maintains 60km/h over predicted horizon.

Figure 4.20 shows the predicted speed trajectories of leading vehicle along with its actual speed trajectory for the case in Section 4.2.3 where observer is used.

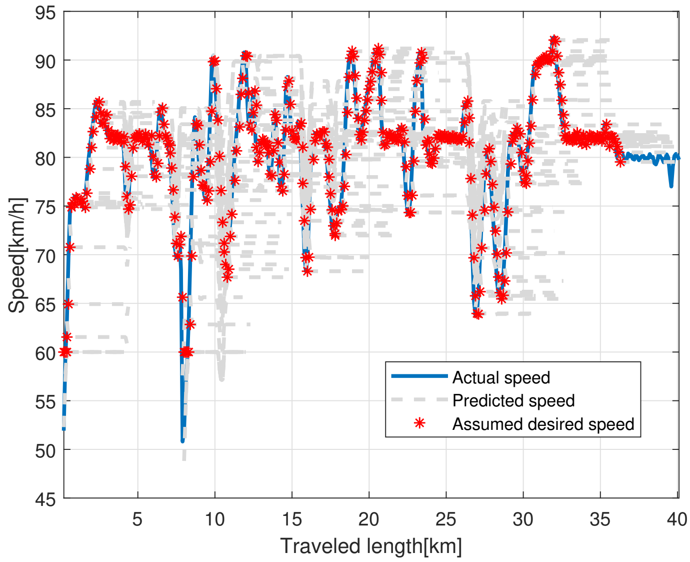

Figure 4.20: The predicted speed trajectory and the assumed desired speed of the leading vehicle for each sample along with the actual speed trajectory when observer is used.

Compared to Figure 4.19, the predicted speed trajectories are closer to the actual speed trajectory which is shown at some instances such as around 16km and 27km.

However, most of the predicted trajectories still do not align with the actual trajectory. The main reason is likely that the desired speed of leading vehicle has been wrongly assumed, and not because of the acceleration limit has been poorly estimated. The observer seems to give a good estimation of the limit just after leading vehicle has driven 1km which is seen in Section 4.2.1. Since the road topography mainly includes downhills, some of the predicted speed trajectories show that the speed is constant over predicted horizon, similar to the case where observer is not available.

4.5 Benefit of HEV

In this section, the benefit of HEV is discussed.

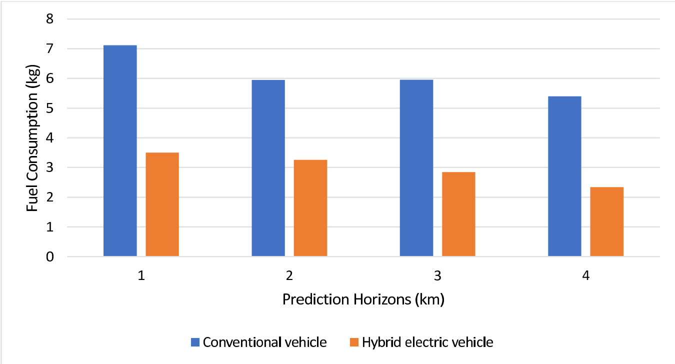

Figure 4.21: Fuel consumption of CV and HEV for different lengths of prediction horizon.

Figure 4.21 shows the fuel consumed by CV and HEV for different prediction horizon lengths. It is shown that the HEV consumes less fuel compared to CV regardless of length of the prediction horizon. As explained earlier, the HEV is able to recover energy by using EM for braking. The energy is stored in the battery and is later used for propulsion of HEV. In addition to this, it also allows ICE to be turned off during certain periods where the EM is able to provide all the necessary power, thus decreasing the fuel consumption further.

4.6 Benefit of having prediction horizon

In this section, the benefit of having different prediction horizon length is discussed. Tables 4.1 and 4.2 show the fuel consumption and final travel time of CV and HEV for different horizon lengths, respectively. From the tables, it can be seen that choosing an optimal prediction horizon length is necessary. When analysing the benefit of prediction horizon length, it is more reasonable to consider the final travel time along with the fuel consumed for each horizon length.

In Figures 4.22 and 4.23, the final travel time and fuel consumed by HEV for different prediction horizons and for the entire road (40.1km) are shown. For the shorter prediction horizons (1-4km), the fuel consumed is higher and it decreases as the prediction horizon length increases. The final travel time does not differ significantly for prediction horizons 1-4km. For the case where the prediction horizon length is set as the entire road, the MPC is run for one update only. It is observed that this case has the lowest fuel consumption, but also the highest final travel time. The reason is that the speed of leading vehicle is predicted lower than its actual speed. Therefore, the host vehicle drives significantly slower, resulting in longer travel time.

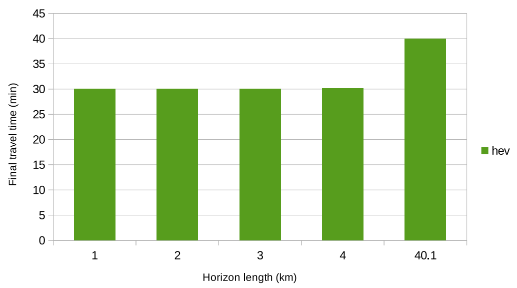

Figure 4.22: The final travel time of HEV for different horizons and for the entire road (40.1km).

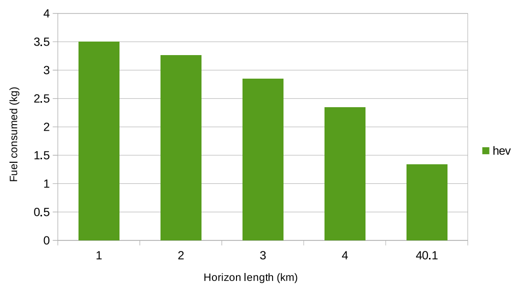

Figure 4.23: The fuel consumed by HEV for different horizons and for the entire road (40.1km).

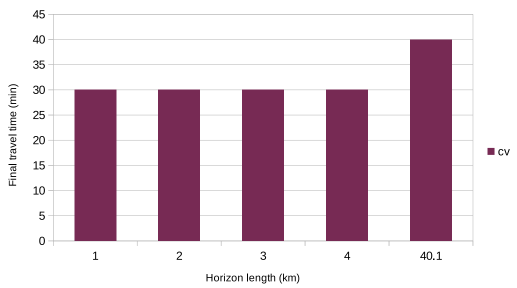

Figure 4.24: The final travel time of CV for different horizons and for the entire road (40.1km).

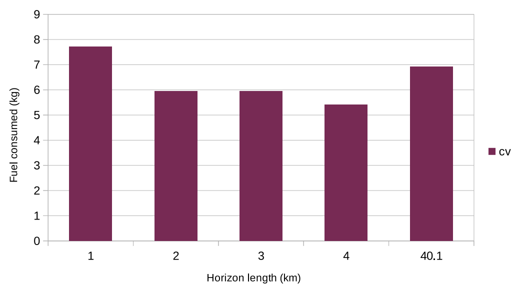

Figure 4.25: The fuel consumed by CV for different horizons and for the entire road (40.1km).

The fuel consumption is lowest since ICE remains off for longer periods compared to the other horizons as EM can deliver the demanded force needed for the host vehicle to drive with lower speed.

In Figures 4.24 and 4.25 the final travel time and fuel consumed by CV for different prediction horizons and for the entire road (40.1km) are shown. It is observed that fuel consumption and final travel time behaviour for prediction horizon lengths 1-4km of CV are similar to HEV. But for the case where the prediction horizon is set as entire road length, the travel time is same but fuel consumption behaviour is quite different from the HEV. For CV, it has to maintain lower gear trajectory as it requires more frictional force by the engine to maintain lower speed, leading to higher fuel consumption.

5
Discussion

This Chapter includes discussion of the results, but also different areas of the work are discussed and how they can be improved for future work.

5.1 Leading vehicle observer and speed prediction

As seen in Figure 4.7, the estimation of acceleration limit gets better for the limits where leading vehicle has driven further as more data has been collected. However, more collected measurement data does not necessarily mean that it gives better estimation as it can also introduce more noisy measurement points which will affect the estimation negatively if noise-counters miss them.

For leading vehicle speed predictor, it has to be assumed that the desired speed of leading vehicle is known. As for the real measurement data, the desired speed of leading vehicle was unknown. As it was also unknown what the maximum allowed speed was for the road, the desired speed was simply assumed to be the average of the collected measured speed during each MPC-update or minimum 60km/h. This greatly influences the results as even if the observer makes a good estimation of the acceleration limit, the prediction can still be bad if the desired speed is guessed poorly. For example, if the actual desired speed is lower than the assumed one, the risk is greater that the host vehicle collides with leading vehicle. If the desired speed of leading vehicle is set as lower than the actual one, host vehicle might drive slower than it should. Knowing the maximum allowed speed of the road would be beneficial, as that could give a hint of what speed leading vehicle wants to maintain. The desired speed could instead be calculated as the average value of the collected measured speed or the maximum allowed speed.

The benefit from using observer is explained in Section 4.4. It is indicated that using an observer improves the leading vehicle speed prediction compared to not using it. This leads to reduced energy consumption and less usage of service brakes. In addition, the safety constraint is less violated when using the observer. However, measurement data of road topography with more uphills is needed to further validate the observer.

5.2 Measurement data and road topography

As mentioned earlier, the road topography mainly includes downhills, which is likely the main reason for the huge fuel reduction for HEV, regardless of horizon length. As there are mainly downhills included, the observer is also less useful for this kind of topography. If topography mainly consisted of uphills however, it would have been more unlikely for the leading vehicle to maintain its desired speed and an observer would then be more useful.

The length of road used for the driving scenarios is also significantly shorter than what a truck normally drives. Measurement data of trucks driving on longer road would therefore be more beneficial to further validate the control algorithm.

For this thesis, it is assumed that the only traffic on the road is the leading vehicle. However, we are not certain of whether there were other obstacles that might affect the driving behaviour of the leading vehicle or not with this measurement data, although it is likely to be the case.

5.3 Choice of prediction horizon

As discussed in Section 4.6, choosing optimal prediction horizon length is necessary. The shorter prediction horizon and the entire road length as the prediction horizon length are not the optimal choice which is shown in Section 4.6 in detail. When choosing the optimal prediction horizon length, it is necessary to compare the parameters such as fuel consumption, final travel time and the safety constraint (t_{sum}) as shown in Tables 4.1 and 4.2. Other parameters such as type of host vehicle (HEV or CV) and the road topography also influence the choice of prediction horizon length. Another thing to point out is that the mass was set as 40ton for both CV and HEV. In reality however, an HEV might be heavier as it includes both electric machine and battery, adding additional weight to the vehicle.

5.4 Ethic and sustainability

By successfully implementing this kind of control algorithm, better fuel efficiency can be achieved. Increased fuel efficiency reduces fuel consumption which means less emission of greenhouse gases to the environment [5][3]. This would also be a big step for autonomous driving as not only would it be able to reduce the fuel consumption, the vehicle would also be able to avoid collision without the need of a driver. The economic cost would then eventually be reduced in the transport business. However, this will also lead to an increase of unemployment for the drivers who may need to apply for other jobs [27].

5.5 Future work

In this section, several aspects are discussed to describe how the work can be improved in future.

5.5.1 Measurement data

Another set of measurement data where the road topography consists of more uphills is needed to further validate the control algorithm.

A more proper and general solution for reducing the impact of noise when measurement data is collected is needed. Other filters such as Kalman Filters and Moving average filter had been tried during the work, but in the end Savitzky-Golay Filter was the one that gives best performance for the given measurement data. Though reducing the impact of noise is crucial, it was not the main topic in this project.

5.5.2 Computation time

The computation time was not considered for this work. Despite this, it is an important factor when it comes to application of MPC. The computation time of developed MPC-algorithm for this thesis can be significantly reduced. Originally, another solver for energy management was intended to be used as well which was much faster than the one used for the results. For the results, the control horizon length was set the same as the prediction horizon length. If a shorter length of control horizon was chosen, the computational time could be further reduced as well.

5.5.3 Model and optimization controller

The power management can be further optimized by changing the power split. Creating a set of feasible F_{M}-points and calculating Hamiltonian cost for each of them is time consuming and might even miss to include a value that is even more optimal than the others. A solution is to find an expression of derivative of Hamiltonian in regards to F_{M} which would likely decrease the computation time for solving the problem in power management.

5.5.4 Road traffic and environment

Only one leading vehicle in front was considered as traffic in the driving environment. In a real scenario though, there is a possibility that multiple leading vehicles are ahead of the host vehicle, making the prediction of its velocity trajectory more complicated.

Another interesting scenario to investigate is to control a platoon of vehicles instead of one single host vehicle, similar to what was done in previous thesis [11], but now with a leading vehicle ahead which is not controlled.

It could also be interesting to investigate the same driving scenario with a leading vehicle, but in a different traffic environment, such as streets and smaller cities. However, the observer would probably not be as useful in those environments as only low speed is usually allowed to be driven, which is very likely to be feasible even for a heavy truck.

6
Conclusion

In this thesis, an MPC-algorithm is developed for an HEV with the purpose of reducing its energy consumption and making sure a safe distance is kept to a leading vehicle. A leading vehicle observer is developed to estimate the power limit of the vehicle which is used to predict its speed and traveling trajectory. The model of HEV, including battery, electric machine and internal combustion engine, was used to formulate the constraints for the optimization problem. Due to the complexity of the optimization problem, the controller solved it in two layers: energy and power management.

Based on the obtained results, it is concluded that the host vehicle (both as HEV and as CV) manages to keep a relatively safe distance to leading vehicle. In addition, the results also indicate that HEV is more fuel efficient than CV. Thus, the control algorithm works as intended.

However, another set of measurement data where the topography has more uphills is needed to further validate the control algorithm and there is still room for improvement in other aspects as well.

Bibliography

[1] *Volvo trucks seeks to accelerate development of more climate-friendly transport*, https://www.volvotrucks.com/en-en/news/press-releases/2019/feb/pressrelease-190219-1.html, 2019.

[2] eurostat, *Modal split of freight transport*, http://appsso.eurostat.ec.europa.eu/nui/submitViewTableAction.do, Retrieved 2018-09-19, 2018.

[3] J. Hirsch, "The environmental impact of long-haul trucking", 2016, pacific standard.

[4] R. Muncrief and B. Sharpe, "Overview of the heavy-duty vehicle market and carbon dioxide-emissions in the european union", 2015.

[5] D. J.-P. Rodrigue, "The environmental impacts of transportation", *The Geography of transport system*, 2017.

[6] *Daf - predictive cruise control.*

[7] *Volvo truck tests a hybrid vehicle for long haul*, https://www.volvogroup.com/en-en/news/2017/feb/news-2476234.html, 2017.

[8] E. Hellström, M. Ivarsson, J. Åslund, and L. Nielsen, "Look-ahead control for heavy trucks to minimize trip time and fuel consumption", 2009, Control Engineering Practice, (17),2, 245-254.

[9] M. N. Lars Johannesson and N. Murgovski, "Look-ahead vehicle energy management with traffic predictions", *IFAC-PapersOnLine*, vol. 48, pp. 244–251, 2015.

[10] L. Johannesson, N. Murgovski, E. Jonasson, J. Hellgren, and B. Egardt, "Predictive energy management of hybrid long-haul trucks", *Control Engineering Practice*, vol. 41, pp. 83–97, 2015.

[11] M. Hovgard and O. Jonsson, "Energy-optimal platooning with hybrid vehicles", Master thesis, 2017.

[12] J. M. Samad Kamal Mazaku Mukai and T. Kawabe, "Ecological driving based on preceding vehicle prediction using mpc", 2011.

[13] Ruchika and N. Ragu, "Model predictive control: History and development", *International Journal of Engineering Trends and Technology*, vol. 4, no. 6, 2013.

[14] M. Ulusoy, *Understanding model predictive control, part 2: What is mpc?*, `https://se.mathworks.com/videos/understanding-model-predictive-control-part-2-what-is-mpc--1528106359076.html`, Retrieved 2018-10-09, 2018.

[15] B. Egardt, “Model predictive control”, Lecture notes 2016/2017, 2017.

[16] S. Boyd and L. Vandenberghe, *Convex optimization*. 2004.

[17] M. S. Thijs van Keulen Bram de Jager, “Optimal trajectories for vehicles with energy recovery options”, 2011, Eindhoven University of Technology.

[18] A. M.A.Hannan F.A.Azidin, “Hybrid electric vehicles and their challenges: A review”, 2014, Renewable and Sustainable Energy Reviews.

[19] D. S. Ahmed M.Ali, “Towards optimal power management of hybrid electric vehicles in real-time: A review on methods, challenges, and state-of-the-art solutions”, 2018, energies review.

[20] T. Nuesch, “Energy management of hybrid electric vehicles”, 2014.

[21] N. Tagner, “Optimal energy management for parallel hybrid electric vehicles using dynamic programming”, Master thesis, 2017.

[22] MathWorks, *Signal smoothing*, `https://www.mathworks.com/help/optim/ug/linprog.html`, Retrieved 2018-10-31.

[23] K. Devleker, *Signal smoothing*, `https://se.mathworks.com/videos/signal-smoothing-97060.html`, Retrieved 2018-10-29, 2014.

[24] MathWorks, *Quadprog*, `https://se.mathworks.com/help/optim/ug/quadprog.html`, Retrieved 2019-03-24.

[25] K. H. Johansson, “Dynamic programming”, Lecture-21.

[26] M. Hogvard, O. Jonsson, N. Murgovski, M. Sanfridsson, and J. Fredriksson, “Cooperative energy management of electrified vehicles on hilly roads”, 2017.

[27] G. D.-C. Tobias Holstein and P. Pelliccione, “Ethical and social aspects of self-driving cars”, 2018.